

U. S. DEPARTMENT OF COMMERCE
WEATHER BUREAU

QC
879.3
.U45
no.5

TEOROLOGICAL SATELLITE LABORATORY REPORT
TO THE
NATIONAL AERONAUTICS & SPACE ADMINISTRATION





114 909

FOR OFFICIAL DISTRIBUTION: This paper has been printed as a manuscript report to the sponsoring agency for the information of selected interested organizations. As this reproduction does not constitute formal scientific publication, any reference to it in published articles and scientific literature should identify it as a manuscript of the U. S. Weather Bureau, Meteorological Satellite Laboratory.

U. S. DEPARTMENT OF COMMERCE

Luther H. Hodges, Secretary

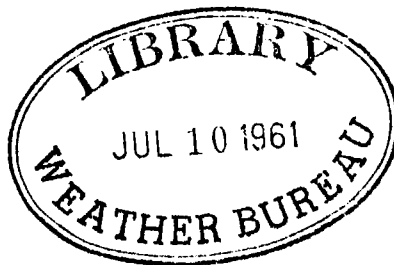
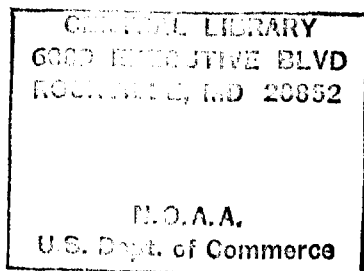
U. S. WEATHER BUREAU

F. W. Reichelderfer, Chief

METEOROLOGICAL SATELLITE LABORATORY REPORT

to the

NATIONAL AERONAUTICS AND SPACE ADMINISTRATION



QC
879.5
.U45
40.5

MSL REPORT NO. 5

TIROS I: CAMERA ATTITUDE DATA, ANALYSIS OF LOCATION ERRORS, AND DERIVATION OF CORRECTION FOR CALIBRATION

by Lester F. Hubert

**Washington, D. C.
April 1961**

114 909

National Oceanic and Atmospheric Administration TIROS Satellites and Satellite Meteorology

ERRATA NOTICE

One or more conditions of the original document may affect the quality of the image, such as:

Discolored pages

Faded or light ink

Binding intrudes into the text

This has been a co-operative project between the NOAA Central Library and the Climate Database Modernization Program, National Climate Data Center (NCDC). To view the original document contact the NOAA Central Library in Silver Spring, MD at (301) 713-2607 x124 or Library.Reference@noaa.gov.

HOV Services
Imaging Contractor
12200 Kiln Court
Beltsville, MD 20704-1387
January 26, 2009

TABLE OF CONTENTS

	Page Number
LIST OF TABLES	iii
LIST OF FIGURES	iv
GLOSSARY OF TERMS	v
ABSTRACT	1
I. INTRODUCTION	1
II. CAMERA AXIS ORIENTATION AND NOMOGRAM FOR PICTURE ORIENTATION	2
III. TIME DETERMINATION BY PHOTOGRAMMETRIC METHODS	12
IV. ANALYSIS OF LOCATION ERRORS	26
ACKNOWLEDGMENTS	40
REFERENCES	41
APPENDIX I. TRANSFORMATION EQUATIONS USED FOR NOMOGRAM CONSTRUCTION	42
APPENDIX II. TIROS I - APPROXIMATED ORBIT AND ASCENDING NODES	45

LIST OF TABLES

		Page Number
TABLE I.	FREQUENCY DISTRIBUTION OF BEGINNING-TIME ERRORS FOR TAPED PICTURES	13
TABLE II.	TIME CHANGE OF NADIR ANGLE ($d\eta/dt$) AS FUNCTION OF TIME FROM MINIMUM NADIR ANGLE FOR VARIOUS VALUES OF MINIMUM NADIR ANGLE (η_0)	20
TABLE III.	COMPARISON OF OBJECT SPACE ANGLES	25
TABLE IV.	PHOTOGRAMMETRIC ORIENTATION FIXES OF TIROS I SPIN AXIS	31
TABLE A.	(Appendix II) TIROS I ASCENDING NODES-TIME AND LONGITUDE	47
TABLE B.	(Appendix II) TIROS I POSITIONS AS FUNCTION OF TIME PAST ASCENDING NODE	59

LIST OF FIGURES

	Page Number
Figure 1. Right ascension and declination of the spin axis, TIROS I.	3
Figure 2. Nomogram for computing azimuth of principal plane and nadir angle of the optical axis	last sheet (unnumbered)
Figure 3a. Perspective sketch of intersection with the celestial sphere of the equatorial plane, orbital plane, and the spin axis.	6
b. Plane of the broken line circle of Fig. 3a showing relation between pp, SAP and ssp.	6
Figure 4. Portion of nomogram showing derivation of angle γ , azimuth of the satellite track, and nadir angle at 38.7 minutes past ascending node at 1156 GMT April 9, 1960.	9
Figure 5. Graph to determine distance on the earth's surface between ssp and pp from nadir angle of the optical axis.	10
Figure 6. Calibration photograph for TIROS I, Camera 2.	15
Figure 7. Drafted copy of calibration photograph for TIROS I, Camera 2.	16
Figure 8a. Measured nadir angles plotted against frame number with line showing a "best fit", pass 116.	18
b. Nadir angles derived from nomogram plotted against time after ascending node of pass 116.	18
Figure 9. Distribution of percent differences between measured $d\gamma/dt$ and theoretical $d\gamma/dt$. Curve "a" uncorrected and curve "b" corrected by regression equation.	21
Figure 10. Nadir angles derived by resection (γ_T) versus nadir angles derived by horizon image measurement (γ_M) and their regression line.	21
Figure i. Spherical triangles involved in transformation of point "X" defined in standard geodetic coordinates to a transverse Mercator map projection. Symbols defined in Appendix I.	44

GLOSSARY OF TERMS

One new term (SAP) has been coined for convenient handling of the subjects treated herein, and several photogrammetric terms are used in a restricted sense. For that reason the following definitions (and their abbreviations where necessary) are listed along with a few other terms that may be unfamiliar to clarify their use in this report.

Ascending node (A.N.): The northbound equator crossing of the satellite.

Azimuth angle: The angle between a directional line on the earth's surface and true north. (Standard meteorological definition).

Declination (δ): Standard astronomical definition.

Nadir angle (γ): The angle measured at the intersection point at the satellite between some specified line and the local vertical.

Object space angle: The angle subtended between two rays in space that intersect at the front nodal point of a camera lens. (Used to differentiate from image space which is between the rear nodal point and the image plane).

Optical axis: The ray perpendicular to the image plane passing through the lens nodal points.

Principal line: The line on the image representing the intersection of the image plane with the principal plane.

Principal plane: The plane determined by the local vertical and the optical axis of the camera.

Principal point (pp): The image principal point is the point of intersection of the camera optical axis with the image plane. The earth principal point is the point of intersection of the optical axis with the earth's surface.

Right ascension (R.A.): Standard astronomical definition.

Spin Axis Point (SAP): The point of intersection with the earth's surface, of the satellite spin axis vector after that vector has been translated parallel to itself to an origin at the earth's center (see figure 3).

Subsatellite point (satellite subpoint) (ssp): Intersection of the local vertical, passing through the satellite, with the earth's surface (i.e., the nadir point).

TIROS I: CAMERA ATTITUDE DATA, ANALYSIS OF LOCATION ERRORS, AND DERIVATION OF CORRECTION FOR CALIBRATION

ABSTRACT

A nomogram is presented along with tabular data for TIROS I orbit to enable users of TIROS I pictures to derive location of the pictures on the earth.

In the course of this data reduction it is frequently necessary to check picture-taking time of the tape-recorded pictures. A photogrammetric method of accomplishing this from the pictures and the nomogram is presented. A systematic error in the camera calibration is shown to influence this time determination and equations to correct this error are derived.

The location errors inherent in the procedures and data are discussed so that users will be able to evaluate the accuracy of mapping various photographed features they may be studying.

I. INTRODUCTION

The high quality of the television images produced by TIROS I has provided meteorological material for research that will undoubtedly be pursued by many different organizations. While picture quality and information content are great, the failure of the system that was to provide orientation of the satellite and the erratic behaviour of the component to provide the time of picture taking, have created serious problems in data reduction. The film available for use by researchers contains something over 20,000 pictures but the plan at this writing is to produce locator grids of latitude and longitude for but a small fraction of the total.

Undoubtedly the requirements for picture locations will increase as more research is started. Many of these requirements will be satisfied by location of the picture center and direction of view of each frame used; others will require complete location of all pictured elements, a task that can be accomplished only by the application of some rectification scheme such as those described by Doolittle, Miller, and Ruff [2] and by Glaser [3]. Any rectification method used, at least in the absence of landmarks, will require the same basic input information, viz. camera orientation in coordinates that can be related to earth and location of the principal point (picture center) or the subsatellite point on the earth.

Section II of this report presents a graphical method by which one can quickly obtain this orientation data in terms of location on earth of the principal point and azimuth of the principal plane. In the process of this data reduction, it turns out that determination of the picture-taking time is a critical step and one beset by difficulties not initially anticipated. Section III of this report considers these problems, and Section IV discusses the errors inherent in the data on which these techniques are based.

II. CAMERA AXIS ORIENTATION AND A NOMOGRAM FOR PICTURE ORIENTATION

The spin axis of TIROS I changed its orientation quite slowly in an inertial coordinate system (Bandeem, [1]) and for that reason axis orientation is conveniently described in terms of right ascension and declination. Figure 1 shows the history of the spin axis orientation from April 1, 1960 to June 15, 1960. The camera axes were parallel to the spin axis and pointed in the opposite direction, so figure 1 represents the coordinates of the camera axes rotated 180° .

In the absence of any other system to provide orientation of the spin axis, photogrammetric methods were employed to derive the data plotted on figure 1. Church's resection method was modified for this task by Doolittle and was adapted to high speed computer use by Miller (Doolittle, et al [2]). This method uses as input data, location of the satellite subpoints as a function of time and the identification of three or more landmarks on the image which are measured in a rectilinear coordinate system superimposed on the image. The output is (a) complete orientation parameters of the optical axis, (b) time of picture taking, and (c) various diagnostic quantities indicating the quality of that particular determination.

Although a majority of the TIROS I pictures did not have adequate landmarks for use in this analysis, approximately 150 frames from 60 different passes provided sufficient data to permit the curves of figure 1 to be constructed; the data points listed in Table IV represent results of the resection analysis. The curves fitted to those points are the result of analysis performed in the Meteorological Satellite Laboratory and represent the best estimate of orientation at this writing. (See discussion of this in Section IV).

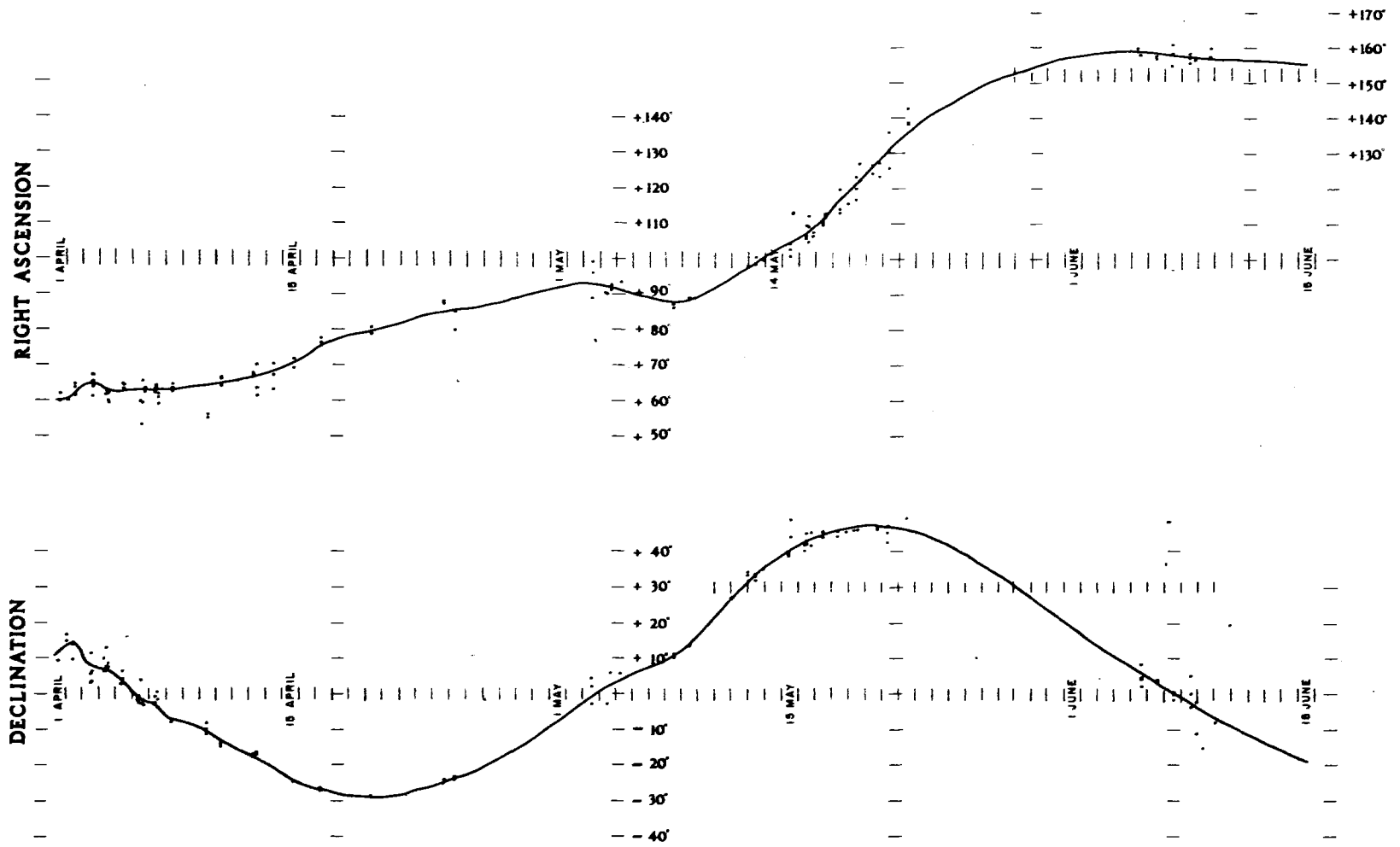


Figure 1. Right ascension and declination of the spin axis of TIROS I.

Nomogram for Application of Orientation Data

The information of figure 1 must be related to coordinates on the rotating earth to be of direct use in mapping of the photographed features. The nomogram constructed for that purpose, figure 2 is based on the spin axis data of figure 1 along with TIROS I orbital elements provided by National Aeronautics and Space Administration.* (Figure 2 is bound as the last sheet of this report so that it can be more easily used).

The principle underlying the nomogram is mapping on the celestial sphere, first, the orbital great circle referred to an origin at the ascending node, and second, a curve representing the intersections of the spin axis with the celestial sphere during the operating period of TIROS I. The relation between the spin axis and the location of the satellite on the orbital circle at the instant of picture taking uniquely determines the camera orientation relative to the earth.

A convenient element to use here is the "Spin Axis Point" (SAP) which is defined in the Glossary of Terms, page v. The longitude of SAP changes with time due to the rotation of the earth, but the latitude is constant as long as the spin axis is unchanged in the inertial coordinate system.

The advantage of using the SAP to describe the orientation of the camera axis relative to the earth is due to the fact that the latitude of the SAP is, for the purpose of this discussion, equal to the declination of the spin axis vector** and the longitude of the SAP can be derived directly from the right ascension of the spin axis by proper application of the Greenwich Hour Angle of Aries.

* Mr. Irwin Ruff of Meteorological Satellite Laboratory devised the nomogram for use during the operation of TIROS I to obtain data needed to plan camera programming. The nomogram has been completely recomputed on the basis of the most complete photogrammetric data available at this writing rather than on the preliminary measurements available to Mr. Ruff during the operation of TIROS I.

**Implicit in this statement is the assumption that declination is equal to geodetic latitude, while actually it is equal to the geocentric latitude. The difference amounts to a maximum of 11 minutes of arc at 45° latitude and therefore is insignificant in this application.

The nomogram is essentially a rectilinear graph with the abscissa representing the orbital great circle on the celestial sphere. This great circle is a straight line here because it has been transposed to a special map projection, particularly suited to this application (a transverse Mercator map projection - see Appendix I).* The curve appearing on the nomogram connects points of intersections of the spin axis with the celestial sphere, to provide a continuous time curve of the spin axis location from April 1 through June 15, 1960.

The right ascension of the ascending node of the orbit and the right ascension of the spin axis changed at different rates. Therefore, in order to construct a single nomogram that could be used for all passes, the origin of figure 2 was fixed at the right ascension of the ascending node and the spin axis positions located relative to that origin. Therefore, the nomogram is a map of a "relative" celestial sphere which has no fixed right ascension because its origin changed with time, remaining always at the ascending node of the orbit. The relation between the celestial coordinates of the SAP on this "relative celestial sphere" and the camera coordinates in the geocentric system is illustrated by figure 3.

↑ Left out of this copy.

Suppose the sphere on which the various great circles of figure 3 are drawn is the "relative celestial sphere" for some particular pass, and that we are viewing it from the outside of that sphere in figure 3a. (A singular position when one considers the radius of the celestial sphere!) By illustrating the celestial sphere in this manner the sketch can also be viewed as representing the earth's surface because the subsatellite track and the SAP have the same relationship on earth as do their projections on the celestial sphere.

Consider point t_1 on the orbital great circle, representing the position of the satellite at the time t_1 past the ascending node. The SAP shown on the sketch, having been located relative to that same ascending node, has the proper location relative to the point t_1 . The great circle arc connecting the satellite subpoint (ssp) with the SAP is equal to the nadir angle of the camera axis at that particular time. Furthermore, it is easy to see that the plane of the great circle just mentioned is also the principal plane, and the dihedral angle (γ) between this plane and the orbital plane when added to the azimuth of the orbital plane at that latitude, gives the azimuth of the principal plane. Since the subpoint location and height of the camera are known, the nadir angle (η) of the optical axis and azimuth of the principal plane completely define the camera orientation in earth coordinates for oblique photographs.

* The construction of the nomogram is based on a circular orbit. Were the orbit significantly elliptical the graphical devices would have to be referred to the true anomaly instead of to the ascending node.

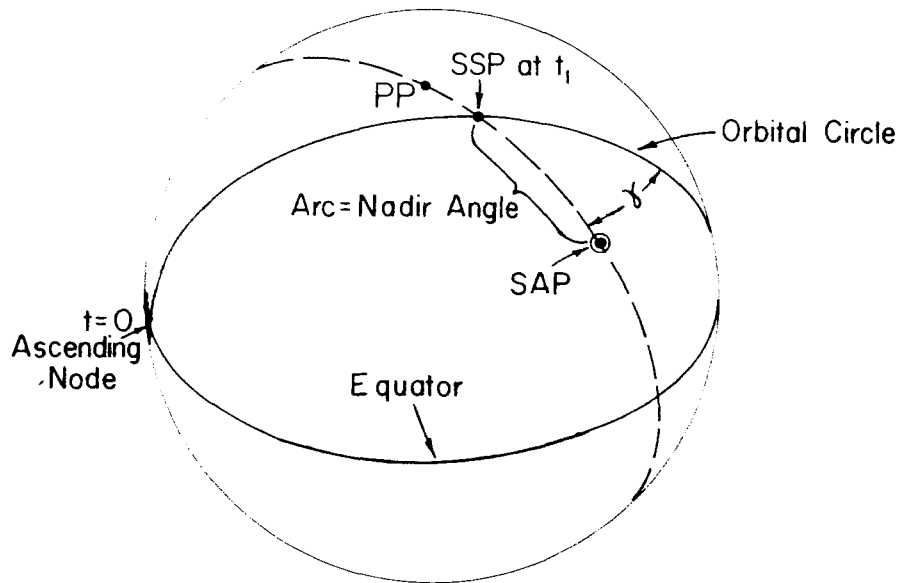


Figure 3a. Perspective sketch of intersection with the celestial sphere of the equatorial plane, the orbital plane and the spin axis. Broken circle is the great circle connecting SAP with a position t_1 on the orbit.

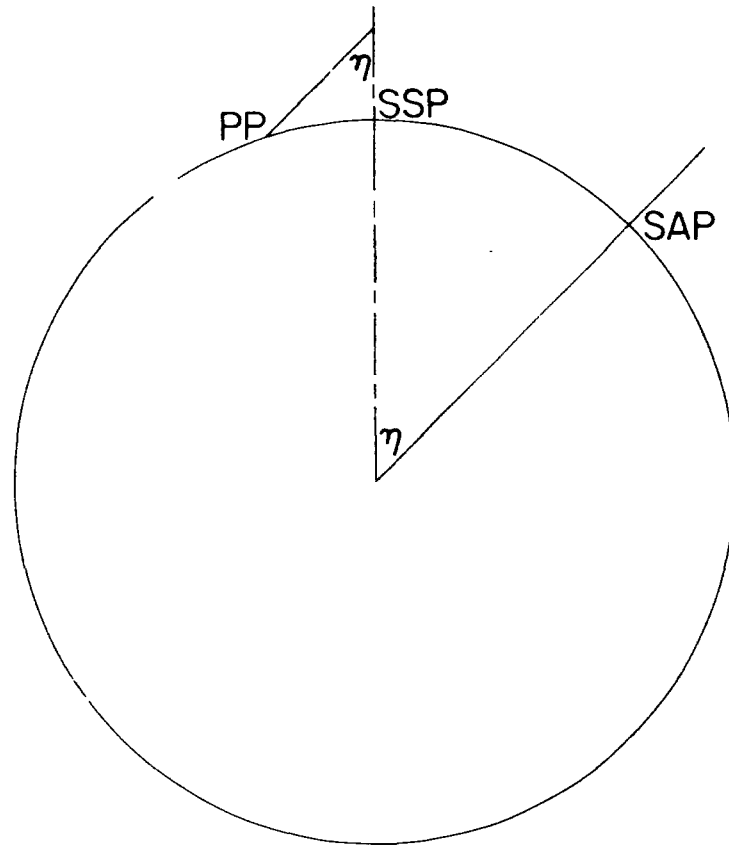


Figure 3b. Plane of the broken line circle of figure 3a showing relation between pp, SAP, and ssp.

The nomogram is designed so that the angle δ and γ can be accurately measured for any desired time and on the same time scale the azimuth of the orbital track is plotted for convenient addition to the measured angle δ . The procedure for using the nomogram to obtain orientation of oblique photographs is shown below with an example illustrating each step. Vertical photographs (in which the optical axis lies along the local vertical) present a different orientation problem because the ssp and pp are coincident and an azimuth of the principal plane cannot be defined. In those cases the orientation must be defined by use of the roll angle. Vertical photographs will be encountered very infrequently, but the outline of a method for orienting them follows the discussion below, under the heading "Roll Angle Determination."

PROBLEM: Obtain location of the picture center and direction of view of frame No. 20, remote picture taken on pass 116, readout at Kaena Point on pass 117.

Step 1. Obtain time of picture taking. In the case of "Direct" pictures the time shown in the catalogue of TIROS I film may be used. Time of "Tape" pictures may be inaccurately shown in the catalogue. More accurate time determination must be obtained by photogrammetric means discussed in Section III.

Example: By nadir angle measurement (see example presented in Section III) the time of taking frame 20 is shown to be 38.7 min. after the ascending node of pass 116. Appendix H shows the ascending node of pass 116 at 11^h16^m54^s GMT April 9, 1960, so time of picture taking is 11:55:36 GMT.

- Step 2.** A. Compute azimuth of principal plane from nomogram. If nadir angle is not already computed:
B. Measure nadir angle from nomogram.

Example: Illustrated in figure 4. Lay a straightedge on the nomogram from the Spin Axis curve corresponding to the time of picture taking to the time on the orbit (the abscissa) corresponding to the time-position of the SAP at picture-taking time. Since the SAPs shown in figure 2 have been computed for 1200 GMT for each day, the proper SAP position is interpolated along the curve between 1200 GMT positions; the proper ssp position is interpolated along the abscissa which is labeled in minutes past the ascending node. Figure 4 shows these points as "a" on the SAP curve corresponding to (11:56) GMT April 9, and as "b" on the abscissa corresponding to (38.7) min. past the ascending node.

A. Lay a protractor on the nomogram to measure the angle δ between the orbital track and the line representing the principal plane. Figure 4 shows $\delta = 169^\circ$.

The azimuth of the orbital plane is labeled along the upper scale. The azimuth of the orbital plane at 38.7 min. (interpolated from the upper scale) is 130.7° . The azimuth of the principal plane is thus $(169^\circ + 131^\circ = 300^\circ)$ (clockwise from north).

B. If the nadir angle is not already known, use dividers to lay off the distance between ssp and SAP and read nadir angle on the nadir angle scale. Figure 4 shows this distance to represent 63° .

Step 3. Obtain the latitude and longitude of the ssp at time of picture taking by use of data in Appendix H.

Example: The example presented in Appendix H indicates how to use those data to obtain a ssp for frame 20, pass 116, at 28.7°N , 8.3°W .

Step 4. Plot on a map the location of the ssp and lay off a line at the azimuth of the principal plane. This line represents the intersection of the principal plane with the earth's surface and the principal point will lie on this line at a distance from the ssp, determined by the nadir angle. This distance can be obtained from figure 5 or computed from equation (1). Figure 5 is computed on the basis of a mean satellite height of 390 n. mi. and an earth radius of 3438 n. mi.

$$\theta = \sin^{-1} \left[\frac{S}{R} \sin \eta \right] \quad (1)$$

where

θ = great circle arc on the earth's surface

η = nadir angle

R = earth radius

S = distance from satellite to principal point,

$$= (H+R) \cos \eta - \sqrt{(H+R)^2 \cos^2 \eta - H^2 - 2RH}$$

H = height of camera at time of picture taking

TIROS I- ORIENTATION NOMOGRAM

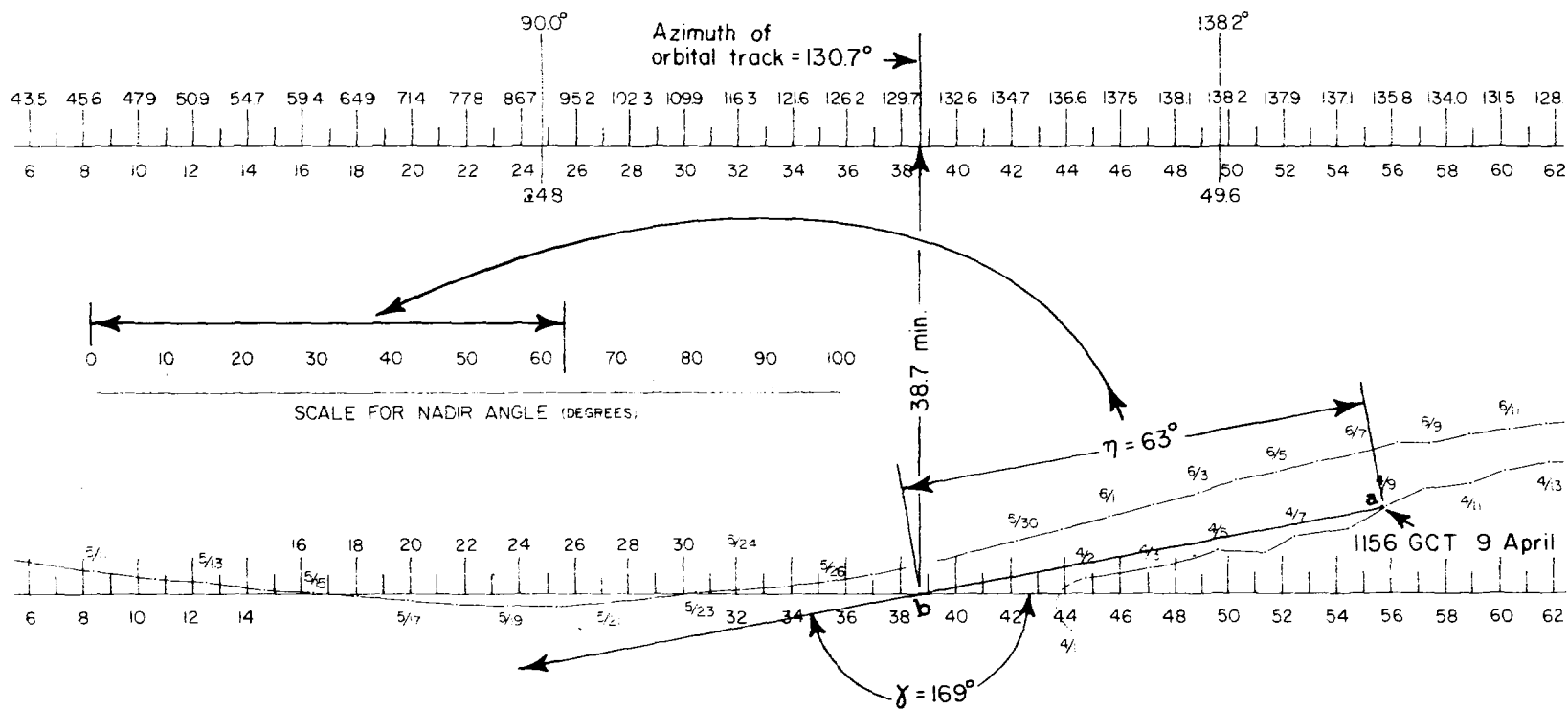


Figure 4. Portion of nomogram showing derivation of angle γ , azimuth of the satellite track, and nadir angle at 38.7 minutes past ascending node at 1156 GMT April 9, 1960.

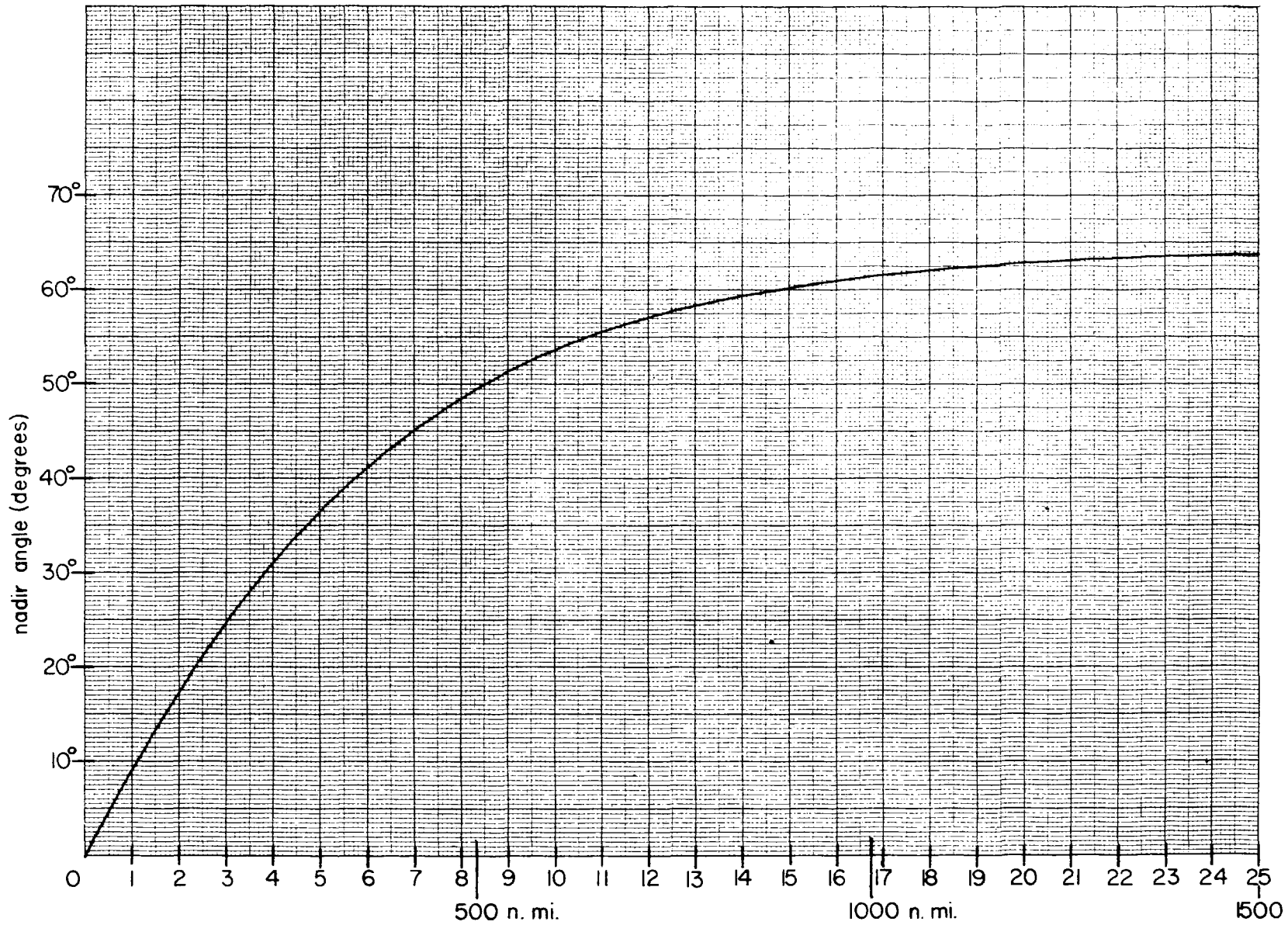


Figure 5. Graph to determine distance on the earth's surface between ssp and pp from nadir angle of the optical axis.

Example: In this particular case the nadir angle is 63° . The angle to the apparent horizon is 64° , therefore, the optical axis of the camera is almost on the horizon. Figure 5 shows the distance from the ssp to the principal point to be 20.4° of great circle arc or 1225 n. mi.

Where the principal point lies on the horizon or above the horizon it is convenient to define an "ersatz" principal point which lies on the earth's surface and more in the foreground. For example we might define the "ersatz" point to be along the principal line at just 35° smaller nadir angle, and use this as a center about which the cloud patterns are plotted. In this example the "ersatz" pp would have a nadir angle of 28° ($63^\circ - 35^\circ = 28^\circ$). Figure 5 shows this point to lie 3.6° of arc from the ssp or 216 n. mi. This point can be easily located on the picture by use of the calibration photograph because the "ersatz" principal point will be at the intersection of the principal line and the outer circle of figure 6.

Roll angle determination

The image principal line is orthogonal to the horizon image and passes through the principal point. The angle between the principal line and some designated axis fixed on the picture format is defined as the roll angle. Since the TIROS cameras rotate about their optical axes, the roll angle of a picture depends upon the rotational position of the camera at the time of picture taking.

On pictures where the horizon is imaged, the roll angle is readily apparent as is the orientation of the photograph relative to the line laid off on a map in Step 4, above. During periods when the spin axis is in the orbital plane (or very nearly in the plane) the entire image is sometimes occupied by the earth's surface and it is not possible to determine the principal line from the image. Furthermore, when the spin axis is in the orbital plane there is an instant in each pass when the optical axis lies along the local vertical, the subpoint and principal point are coincident, and no "principal line" is defined. Under these conditions it is necessary to establish compass directions on the picture in order to orient it on a map.

The picture-taking intervals are usually 30 seconds and the spin rate was constant for any one sequence so that it would seem that the roll angle between pictures could be easily computed and each picture could then be laid down with predetermined angle between them. Experience has shown that this is not a practical procedure, probably because the picture interval varied by a fraction of a second. The spin rate was about 10 r.p.m. (60° per second) so a very small irregularity in the interval could produce significant changes in the roll angle from picture to picture.

The most direct and accurate method of determining roll angle for frames on which the horizon or recognizable landmarks do not appear is by use of cloud patterns common to adjacent pictures. The orientation of several cloud patterns is established on pictures where the horizon is visible, and the adjacent pictures that show the same clouds are orientated in such a way that the cloud patterns retain the correct orientation. Clouds common to that picture and the following ones are then matched, and so on through the sequence.

III. TIME DETERMINATION BY PHOTOGRAMMETRIC METHODS

Why is time determination necessary?

TIROS I, being a spin stabilized vehicle, continuously changed its orientation relative to the earth. The optical axis of the camera was directed earthward at one moment in each pass and toward space 50 minutes later. Therefore, in order to map the photographed features of any one "snapshot" it is necessary to know at the time of picture taking, (a) the three-dimensional position of the camera, (b) the orientation of the camera's optical axis, and (c) the roll position of the camera (viz. which direction of the picture is "up").

Requirement "a" is fulfilled by the NASA orbital data which is provided in the form of latitude and longitude of the satellite subpoint at minute intervals and the satellite height at those positions.*

Requirement "b" is available, as a function of time, and has already been discussed in Section II.

Requirement "c" (apparent directly from all pictures in which the horizon is visible) has also been discussed in Section II.

It is therefore clear that the best possible estimate of picture-taking time is necessary because the orientation data of "a" and "b" are known only as functions of time.

What time error is involved?

When the pictures were taken in response to direct commands from the interrogation stations, time was accurately recorded by ground-based equipment, but pictures taken remotely and stored on tape had no such accurate time record.

* These data have been generalized and tabulated in Appendix II. For the purpose of picture location, tabulations in Appendix II, and the mean height of 390 n. mi. fulfill requirement "a".

The remote picture timing depended upon (a) a time-delay register on the satellite set by command from the ground, (b) a pulse generator on the satellite to count the delay time, and (c) a pulse generator on the satellite to trigger the shutter at 30-second intervals.

It became apparent early in the operation of TIROS I that operations (a) and (b) were somewhat erratic because pictures were not always taken at the programmed times. Step (c) was better behaved because even at this writing there is no conclusive evidence that the picture taking interval was in error by more than a fraction of a second. Table I is a tabulation of a small random sample of beginning-time errors compiled to illustrate the order of errors involved.

TABLE I. FREQUENCY DISTRIBUTION OF BEGINNING-TIME ERRORS OF TAPED PICTURES

Time Error	Number of Cases	
	<u>Started early</u>	<u>Started late</u>
0 to 0.5 min.*	5	1
0.6 to 1.0 min.*	8	1
1.1 " 1.5 "	3	1
1.6 " 2.0 "	3	0
2.1 " 3.0 "	0	2
3.1 " 4.0 "	1	0
4.1 " 5.0 "	1	0

If one assumes that Table I represents typical errors, it follows that nearly a third of the remote pictures were taken at least 2 minutes different from the programmed times. A time error of 2 minutes produces a location error of 435 n. mi. even if all other variables are known exactly.** Furthermore, the possibility that any picture might involve a 5-minute error, requires that times be checked where it is necessary to map photographed features within a few hundred miles of their true position.

* Accuracy of time determination is little better than a minute so all cases listed in the first two classes must be considered as "no error".

**It should be borne in mind that this discussion applies to pictures which show no recognizable landmarks so that mapping depends entirely upon the orientation data.

Measurements on TIROS I Images for Photogrammetric Application

The purpose of making measurements on images is to derive object space angles formed by rays from various objects to the front nodal point of the lens. Due to the fact that the television system of Camera 2 has nonlinear electronic distortions superimposed on a large "barrelling" lens distortion, a convenient method of converting image distances to object space angles is by use of the calibration photograph of figure 6 (Staff members R.C.A., [5]). That photograph of a polar diagram was made through the entire television system before launch by setting up a target so that the concentric circles subtended known object space angles from the camera. An image from TIROS I Camera 2 can thus be superposed on that calibration target, and object space angles read directly. It is only necessary to adjust the photograph size to the size of the calibration photo, and this can be done by use of the fiducial marks.

On TIROS I pictures are fiducial marks that, when visible against a light background, show up as four corner "L's" and a center "+". Figure 7 is a drafted copy of the image of figure 6 on which the fiducial marks are clearly marked.

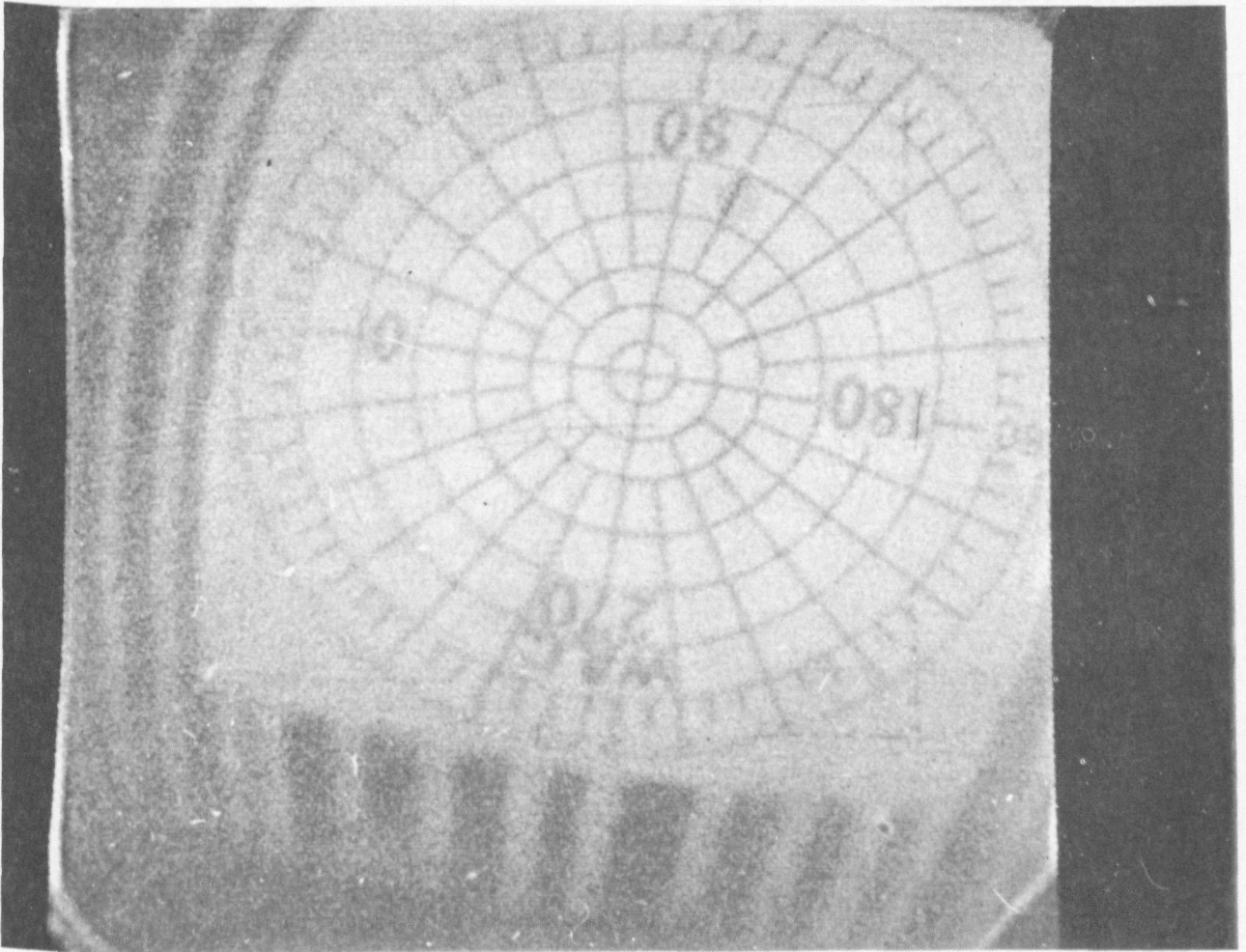
The center of the polar target is the principal point of the picture.* Since the polar diagram does not appear on any of the cloud photographs, it is necessary to locate the principal point of each photograph by measuring off the proper distance from the center "+", and object space angles are then computed by measuring image distance from that point.

Time Determination by Nadir Angles

The nadir angle of the ray from the horizon, regardless of camera orientation, is dependent (for a spherical earth) only upon the height of the camera and the elevation of the apparent horizon above sea level. It has been shown that the latter can be neglected for the purpose of this discussion (Hubert, [4]). In the reference just cited, it is also shown that the nadir angle of the optical axis can be derived from the position of the horizon curve on the image, where object space angles can be derived from image distances.

* **IMPORTANT CAUTION:** Care must be exercised to orient the picture right side up before locating the principal point relative to the center "+". "Right side up" is different for "Direct" and "Tape" pictures. Figures 6 and 7 are labeled both "Direct" and "Tape". When using "Tape" pictures turn the targets so that the film legend and the word "Tape" correspond, and when direct pictures are used, rotate 180° so that the film legend and the label "Direct" correspond.

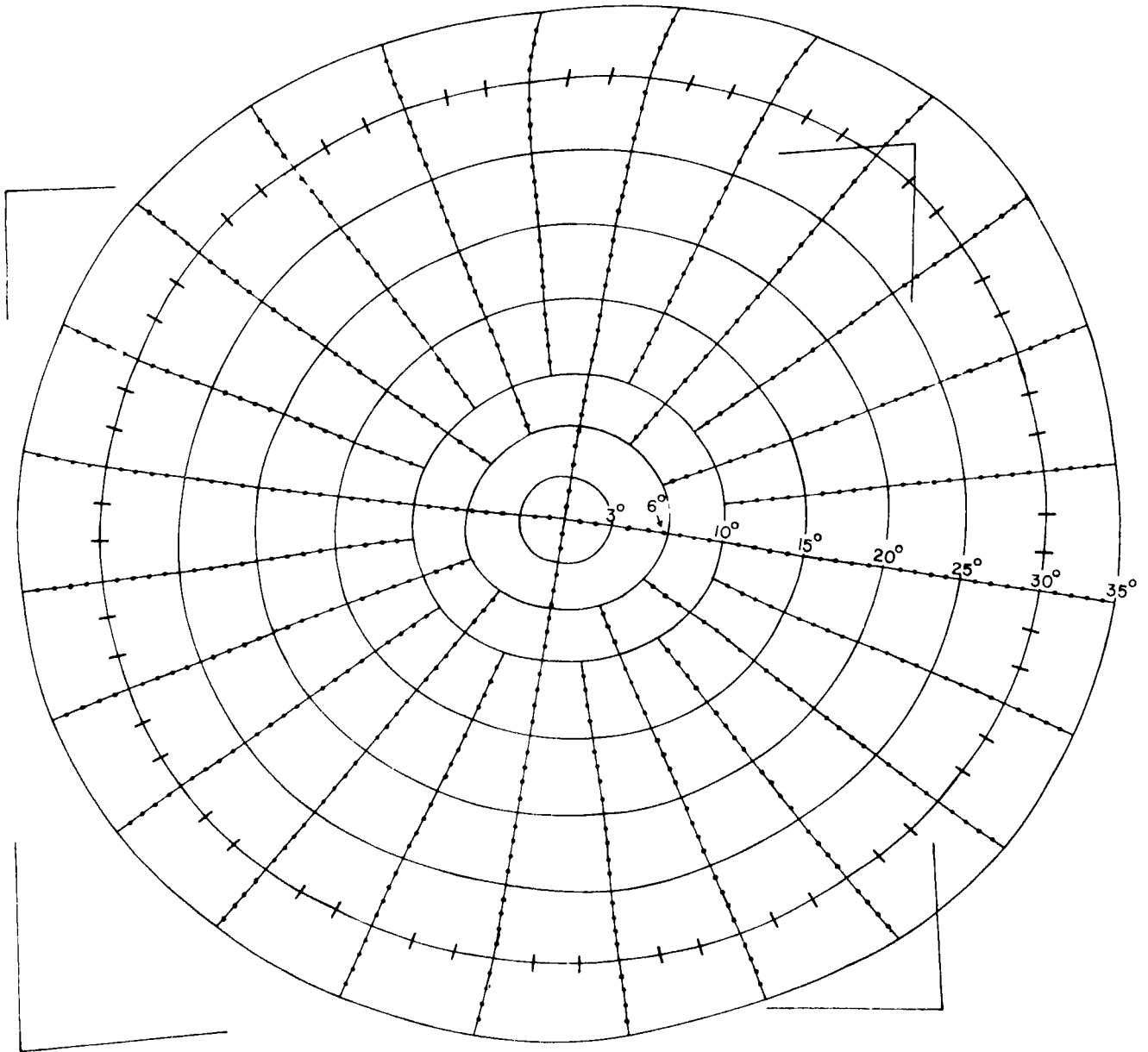
TAPE



DIRECT

Figure 6. Calibration photograph for TIROS I, Camera 2.

TAPE



DIRECT

Figure 7. Drafted copy of calibration photograph for TIROS I, Camera 2.

The broad field of view of Camera 2 provided an image of the horizon on a majority of the pictures. Therefore, the nadir angle of the optical axis can be derived for a majority of the wide angle pictures. The nadir angle of the optical axis is a unique function of camera orientation and location of the satellite subpoint, and these in turn, are known functions of time. Time determination can thus be made by (a) measuring a series of nadir angles and plotting the sequence of angles versus frame number, (b) plotting a series of nadir angles from orientation data as a function of time, and (c) matching these curves to associate frame number with time.

An example is shown in figure 8. Figure 8a is a plot of the measured nadir angles on the sequence from pass 116 and readout on pass 117 at Kaena Point, Hawaii, April 9, 1960; the line is an eye-fitted straight line to the measured angles. Figure 8b shows the nadir angles computed from the orientation data, plotted as a function of time, with the origin the time of minimum nadir angle, expressed by equation (2)

$$\eta = \cos^{-1} \left(\cos \eta_0 \cos \frac{2\pi t}{P} \right) \quad (2)$$

where,

η = nadir angle of the spin (and optical) axis

η_0 = minimum nadir angle

P = orbital period = 99.2 min.

t = time measured from time of the minimum nadir angle

The nomogram, figure 2, shows both the minimum nadir angle and the time of that minimum past the ascending node. Therefore, the plot of nadir angle versus time can be made by reading values from that graph instead of using equation (2).

In this example, $\eta_0 = 11^\circ$ and the angles η for times from 31 to 56 min. past the ascending node are shown. Matching the nadir angles between figure 8a and 8b yields the time of picture taking. For example frame 20 with a nadir angle of 63° corresponds to 38.7 min. past the ascending node of pass 116. There exists in figure 8a however, a systematic error that must be compensated before correct picture-taking times can be found for all pictures, but the above example was chosen so this particular time remains unchanged by the correction discussed below.

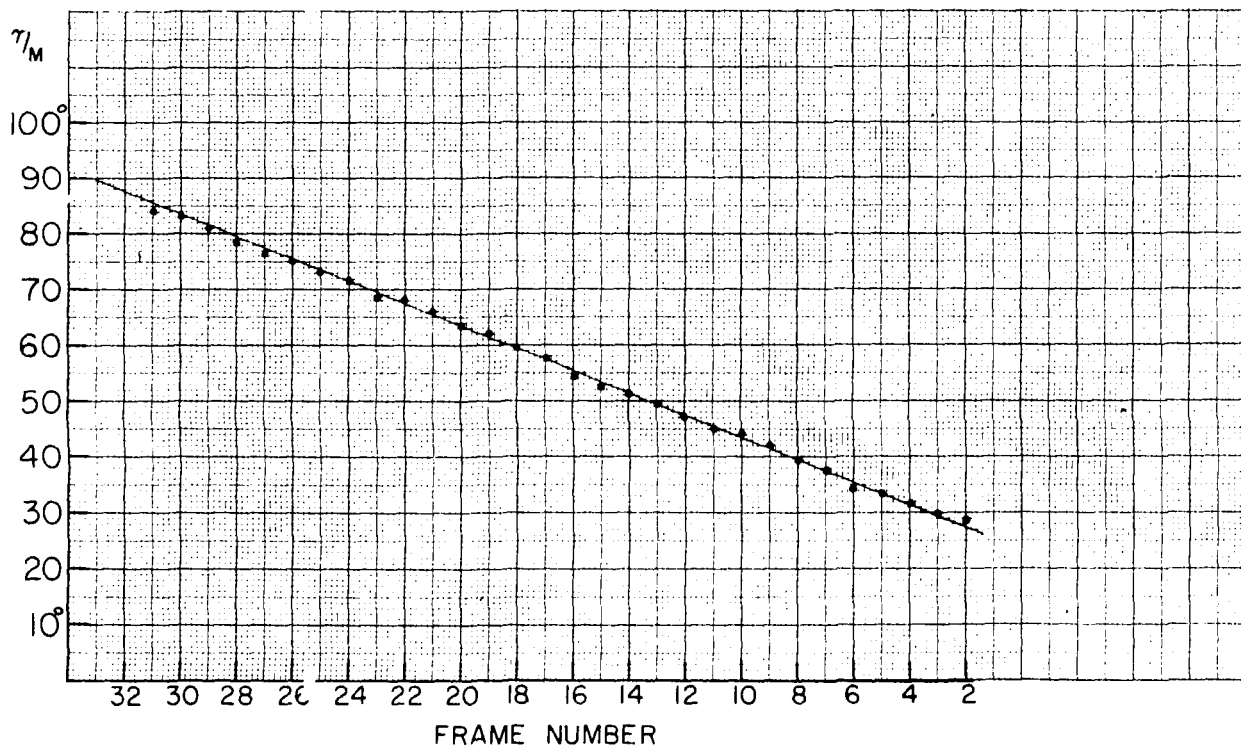


Figure 8a. Measured nadir angles plotted against frame number with line showing a "best fit", pass 116.

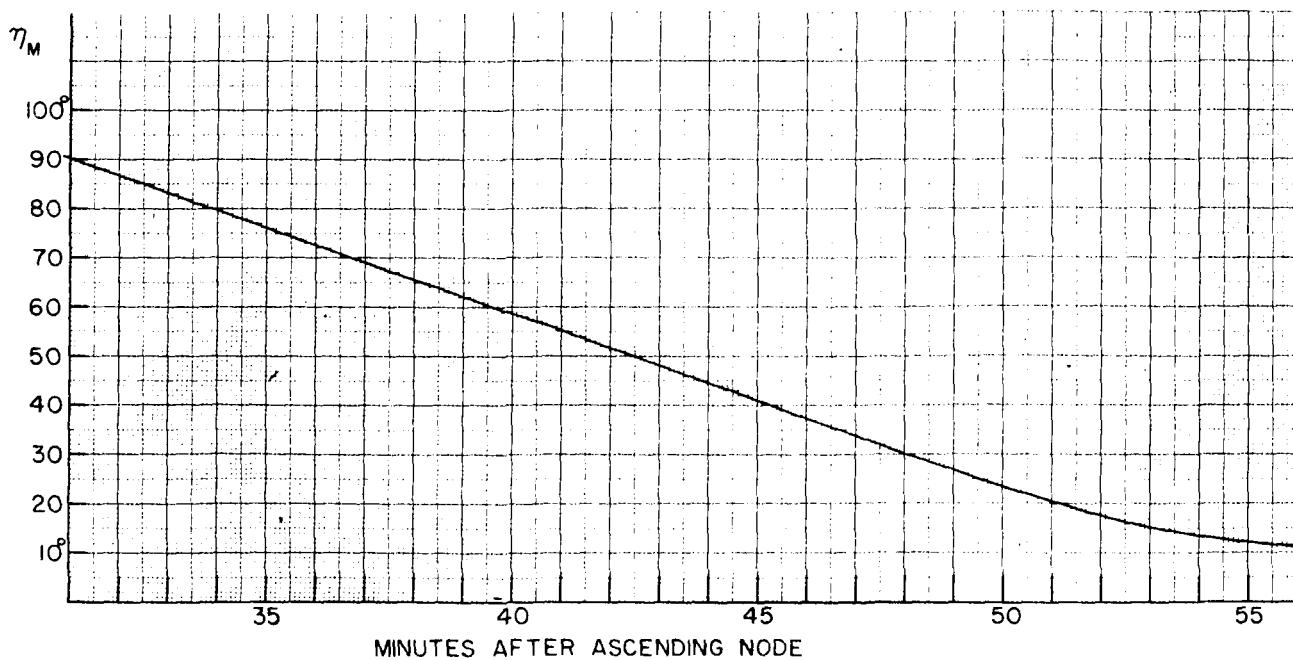


Figure 8b. Nadir angles derived from nomogram plotted against time after ascending node of pass 116.

Correction for a systematic error in nadir angle determinations

The Meteorological Satellite Laboratory set up a program to determine the time of many remote picture sequences by the method outlined above. After a large number of angles had been plotted it was found they did not agree with the angles derived by the resection method. The diagnosis of this source of error and derivation of the correction equation is described below because users of TIROS pictures will thereby gain insight into the types of uncertainties that influence mapping of pictured features.

The two methods of obtaining nadir angles (resection and horizon angle) are largely independent because the measurements are performed independently and by different methods. But more important, the resection program depends upon "x" and "y" measurements on a superimposed rectilinear coordinate system of a minimum of three image points well below the horizon, while direct measurement of the angle to the horizon depends upon a single image distance. The problem was to establish which set of nadir angles is most accurate and to derive a correction equation. It would appear that the method which depends upon a single measurement (and frequently to the extreme edge of the image) is more vulnerable to error than the resection method which uses several measurements on each picture. Nevertheless it was not possible a priori to proceed on that assumption.

Because horizon images are visible on a large number of pictures in each taped sequence, it was possible to utilize the time-rate of nadir angle change in this investigation. Differentiation of equation (2) yields,

$$\sin \eta \frac{d\eta}{dt} = \frac{2\pi}{P} \left(\sin \frac{2\pi t}{P} \right) \cos \eta_0$$

and when the optical axis is in the orbital plane,

$$\cos \eta_0 = 1 \quad \text{and because } \sin \eta = \sin \frac{2\pi t}{P}, \quad \frac{d\eta}{dt} = \frac{2\pi}{P} = \text{Constant}$$

When the optical axis is not in the orbital plane the nadir angle time-rate near the time of minimum nadir angle is not constant but for most other times it changes only slowly. Table II lists the time-rates for various minimum nadir angles which cover the range for TIROS I.

TABLE II. TIME CHANGE OF NADIR ANGLE ($\frac{d\eta}{dt}$) AS FUNCTION OF TIME FROM MINIMUM NADIR ANGLE (t_0) FOR VARIOUS VALUES OF MINIMUM NADIR ANGLE (η_0)

	<u>Time Interval</u> <u>$\pm (t-t_0)$</u>	<u>Average</u> <u>(deg. min⁻¹)</u>
$\eta_0 = 0^\circ$	All time intervals	3.62
	0 to 2	1.90
$\eta_0 = 5^\circ$	2 to 4	3.25
	4 to 6	3.55
	6 to 50	3.60
	0 to 2	1.15
$\eta_0 = 10^\circ$	2 to 4	2.60
	4 to 6	3.15
	6 to 12	3.40
	12 to 50	3.50
	0 to 2	0.90
$\eta_0 = 15^\circ$	2 to 4	2.10
	4 to 6	2.70
	6 to 12	3.30
	12 to 50	3.40
	0 to 2	0.60
$\eta_0 = 20^\circ$	2 to 4	1.65
	4 to 6	2.40
	6 to 12	3.10
	12 to 50	3.20
	0 to 2	0.60

The measured nadir angles were plotted and the values of $d\eta/dt$ compared with the values obtained from equation (2). Figure 9 curve "a" shows the frequency distribution of differences between the computed rate and the measured rate. The measured values were, on the average 11% greater than the computed rate. Curve "b" represents the same frequency distribution after a correction equation had been applied to the measured sequences. The corrections were derived as follows.

The hypothesis was made that the resection method produced a good estimate of the true nadir angle. For all pictures analyzed by that method, the nadir angles were also derived from horizon measurements and a regression equation computed (98 pairs). Figure 10 is a plot of "true" (resection) nadir angles against "measured" angles and the regression line is shown as a broken line on that figure. The equation is:

$$\eta_T = 6.4 + 0.90\eta_M \quad (4)$$

where η_T = "true" nadir angle
 η_M = "measured" nadir angle.

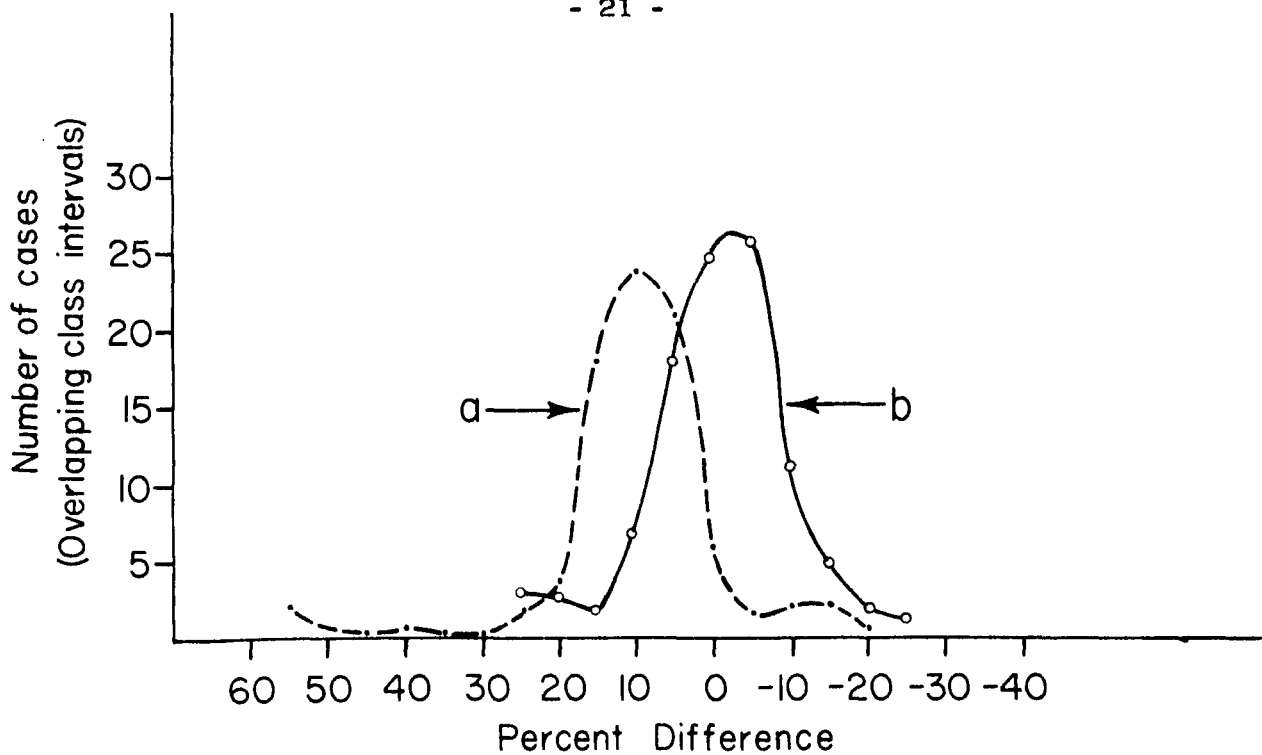


Figure 9. Distribution of percent differences between measured $d\eta/dt$ and theoretical $d\eta/dt$. Curve "a" uncorrected and curve "b" corrected by regression equation.

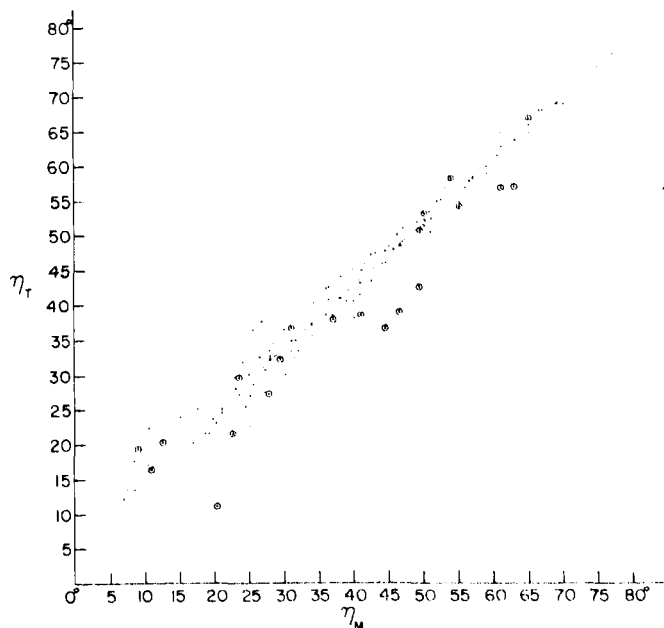


Figure 10. Nadir angles derived by resection (η_T) versus nadir angles derived by horizon image measurement (η_M) and their regression line.

The circled points of figure 10 have not been included in the regression line computation because the resection analysis yielded internally inconsistent orientation values for the spin axis. These inconsistencies were probably due to non-compensated distortions in the system and/or landmarks that subtended very small object space angles--a condition that rendered the resection extremely sensitive to slight measurement errors.

Using equation (4), the sequences of measured nadir angles were corrected and the corrected values of $d\eta/dt$ were compared to the computed slopes. The result is illustrated in curve "b" of figure 9, already mentioned. The fact that this corrected distribution exhibits the proper value of $d\eta/dt$ is strong evidence that equation (4) should be applied to measurements of nadir angle based on D-3 calibration photograph (Staff, R.C.A., [5]).

Correction for Object Space Angles

The regression for correcting nadir angles can be transformed into an equation for correcting object space angles by a simple translation of origin, and in this form is more useful for making image measurements for various photogrammetric application.

The nadir angle to the apparent horizon from a mean height of 390 n. mi. is 64.0° . Therefore, when the horizon image passes through the image principal point, the nadir angle of the optical axis is 64° , and the object space angle between the optical axis and the ray to the horizon is zero. The origin of the regression equation (4) was therefore translated to the point $\eta_M = \eta_T = 64^\circ$, and equation (4) becomes, $\theta_T = 0.90 \theta_M$

where, θ_T = true object space angle (measured from principal point)
 θ_M = measured object space angle (measured from principal point)

Source of Angle Measurement Error

The regression equations (4) and (5) have been derived from the analysis of 98 TIROS I photographs. In order to apply with confidence the corrections based on this small sample, it is desirable to identify the cause of that error in order to decide whether the corrections should be applied to all TIROS I pictures.

The question to examine is "Do the discrepancies arise because there is a basic error in the calibration photograph, figure 6?" In the following discussion it is shown that it is highly probable the calibration diagram is in error by the amount indicated by the regression equation.

Because the excessive rate of nadir angle change ($d\eta/dt$) was used as prime evidence in the above, let us consider how this bias could have been produced.

Time-rates were computed from finite differences, assuming that,

$$d\eta/dt = \frac{\Delta\eta}{\Delta t}$$

and it was also necessary to assume that the picture-taking interval (Δt) was a constant, 30 seconds.

It is therefore clear that any of the following three factors or any combination of them, could produce excessive values of $d\eta/dt$.

1. The object space angles estimated by use of the calibration diagram, figure 6, were in error.
2. The picture-taking interval was longer than the pre-set interval of 30 sec.
3. A nutation in the spin axis produced a change of spin axis orientation during each picture-taking sequence.

Nutation. A short period nutation (3 above) can be virtually eliminated by considering the highly improbable events that would have to occur to produce the observed results. If a nutation were responsible for the 11% excessive value of $d\eta/dt$ it must have had a component $0.33^\circ \text{ min}^{-1}$, which was exactly in phase with the picture-taking times, such that the change of angle due to the nutation would be in the same sense as the change caused by rotation of the satellite about the earth. If the phase were not highly correlated in this manner the nutation would produce a dispersion of measured $d\eta/dt$ about the value computed for a fixed axis orientation, but would not produce a significant bias as observed. Such a perturbation component is not unreasonable, but the in-phase relation to picture sequences is unlikely because the sequence beginning time was essentially random within the 30 to 40 minutes of available picture-taking time.

Time intervals. The picture-taking interval of taped pictures (2 above) is shown to be 30 seconds by inspection of the results of the time determination by the resection method. Two and three consecutive frames of many passes were analyzed in this manner, and because picture-taking times were determined independently for each frame, many time intervals were thus a by-product.

The computer program of the resection analysis determined time of picture taking by searching up and down the subsatellite track at points corresponding to 5-second intervals to find the position that corresponded most closely to the three-dimensional camera position derived from the picture resection. Due to experimental errors and non-compensated distortions in the pictures, the time thus determined may easily be in error by 5 to 10 seconds. As a result, the picture intervals sometimes turned out to be 25 seconds and 35 seconds. For each such determination however, there are printed out diagnostic elements that permit one to select the determination which is most accurate. About one-third of all cases were eliminated because they contained significant internal inconsistency, and the remaining two thirds were averaged; the mean picture interval was exactly 30 seconds.

To summarize, an objective selection of the best determination of picture interval by the resection method yielded a sample of 54 intervals which exhibited a dispersion that was inherent in the method, but had a mean of exactly the proper 30 seconds. Therefore, while it is possible that some individual intervals were different from 30 seconds, there is no evidence for an 11% bias that would be necessary to explain the observed values of $d\eta/dt$.

Factors (2) and (3) of the above list have thus been eliminated and the most probable explanation is therefore that angle measurement based on figure 6 caused the excessive measured values of $d\eta/dt$.

How can such an event be explained? Could electronic distortions or a changed adjustment of the receiving monitor between calibration and operation account for the discrepancy?

Examination of pictures produced at the two readout stations suggests it was not due to monitor adjustment. If the calibration were sensitive to monitor adjustment, it is likely that the two readout stations, operated completely independently, would produce pictures exhibiting quite different distortion. The data pairs used to compute regression equation (4) were separated into two sets according to which station had produced them, and regression equations computed for each set. The 41 Kaena pictures yielded an equation,

$$\eta_T = 8.1 + 0.87\eta_M$$

while the 57 Monmouth pictures produced the equation,

$$\eta_T = 6.2 + 0.92\eta_M$$

While this difference may reflect the effect of different monitor adjustments, it is a small difference. For example, a measured nadir angle of 30° would be adjusted to a true nadir angle of 34° by both of the above equations.

The conclusion indicated is that either a deformation of the image-producing system on the satellite occurred between calibration and operation, or there was an error in production of the calibration data. TIROS I is unavailable for recalibration, so the first possibility cannot be investigated. A simple explanation, however, can account for the discrepancy.

The National Bureau of Standards examined the optical system during calibration of the second TIROS (which was identical to the first) and found that the front nodal point of the lens was 1.95 inches behind the surface of the front lens element. In the arrangement of the target for producing the calibration photograph, figure 6, the distance from target to nodal point was to have been 17.0 inches. Had this distance been measured from the front lens surface, the distance from the nodal point would have been 18.95 inches. Table III shows the error that would have been thus produced, and, for comparison, the regression-corrected angles are listed in the last column.

TABLE III. COMPARISON OF OBJECT SPACE ANGLES

<u>Angle of calibration polar target based on distance of 17.0 in.</u>	<u>Actual angle if distance were 18.95 in.</u>	<u>Corrected angle obtained by applying equation (5) to calibration photo angles</u>
10°	8° 59'	9.0°
20°	18° 05'	18.0°
35°	32° 08'	31.5°

The agreement between the last two columns is remarkable considering the opportunity for experimental error in deriving equation (4) and the fact that the relation between "true" and "measured" angles should be non-linear. If the target were set an incorrect distance from the camera, the relation between θ_T and θ_M would be:

$$\theta_T = \theta_M - \frac{\Delta D}{D} \sin \theta \cos \theta \quad (6)$$

where, $\frac{\Delta D}{D}$ = fractional error in distance from node to target.

Equation (6) is very nearly linear in the range of angles involved in the data used, however, so they could not be expected to reveal the non-linearity.

The above result demonstrates that all angles derived by use of the calibration photograph, figure 6, must be corrected by application of equations (5) or (6). Where the object space angles are small, the linear equation (5) and the non-linear equation (6) are quite similar, so that simpler equation (5) may be applied with no practical loss of accuracy. In some applications it may be more convenient to make the necessary correction by adjusting the enlargement size of the photographs by 10%. While this is not strictly correct, the "barrelling" lens distortion tends to compensate for the approximation thus introduced.

Summary of Section III

A small sample of sequence starting times has suggested that some taped pictures may have been taken at times at least 5 minutes different from the programmed times. This implies that it is necessary to check the picture-taking time of each taped sequence showing no landmarks, when it is desirable to locate pictured cloud features within a few hundred miles of their correct position. Time checking is required because the positional variables used in mapping are known only as functions of time.

Time determination utilizes a photogrammetric method involving the calibration photograph, and this in turn, is shown to be in error. A regression equation was derived from empirical data and a plausible explanation for the error was discussed. Based on that explanation a theoretical correction equation was derived. It is necessary to correct all space object angles obtained by use of the calibration photograph, either by use of the derived equations or by any method that produces an equivalent adjustment.

IV. ANALYSIS OF LOCATION ERRORS

The purpose of this section is to assess, insofar as possible, the errors inherent in mapping photographed features by the method described here, where the pictures show no landmarks. It is essential that users of these data acquire an appreciation of the uncertainties involved so they will not be led into unwarranted conclusions based on details of position.

Mapping errors are brought about by:

1. errors in locating on the earth's surface the picture principal point,
2. errors in compensating for image distortion in computing the positions of features about that principal point, and
3. errors in determining the orientation on the image format of the principal line. This is more likely to be a serious error source in pictures with no horizon image, and has already been discussed under "Roll Angle" in Section II.

The errors produced by 2 and 3 above are negligible near the principal point and in the picture foreground, and most serious toward the horizon. The area toward the horizon reveals the least amount of small-scale detail due to decreasing resolution of the television system with increasing distance and due to foreshortening of the high oblique view. Consequently, the principal utility of the background portion of the picture is to delineate large-scale features, and mapping accuracy is less critical than it is in the foreground.

The important mapping errors introduced by the data and techniques presented in this report are due to the principal point location -- and it is only this aspect that is discussed here.

It is not possible to make a rigorous error analysis because some factors have no adequate measurement, either in the calibration or experimental data available at this writing. Considerable experience with the data, however, has led to some good estimates of the range of errors that are inherent in the various elements. For that reason it appeared worthwhile to combine the estimated and measured error components in order to give users a best estimate of the combined effect.

The methods of analysis of variance are applied, and the validity of the result depends upon the implicit assumption that the errors are random, independent, and normally distributed. Also, it is assumed that the estimates of "largest error" (based on experience) represent at least 95% of the error that could exist, so that the "largest error" can be treated as an estimate of two standard deviations.

Accuracy of locating the principal point depends upon the precision with which the following three sets of variables can be specified.

1. Camera position relative to the earth at time of picture taking.
2. Distortion over the image format.
3. Orientation of the optical axis.

The satellite subpoint and height are tabulated for each minute to an accuracy an order of magnitude greater than the items discussed here, so the only significant position error is due to time uncertainty, already discussed in Section III. In that section it has been shown that time determination by the photogrammetric method described depends both upon orientation of the spin axis and distortion of the images. Therefore, items 2 and 3 both introduce uncertainties in camera position via their effect on time determination. Because of this the TIROS I pictures fall into three categories insofar as time errors are concerned. The first category contains the smallest error, the second contains the error of the first in addition to its own, and the last category contains the uncertainties of all three.

- Category I: Time recorded on ground-based equipment (direct pictures).
- Category II: Time determined by the photogrammetric method of nadir angle measurements, orientation known by resection analysis of pictures in that same pass.
- Category III: Time determined by nadir angle measurements, orientation not accurately known because it has been interpolated from the curves of figure 1.

Evaluation of Time Errors Which Produce Camera Position Errors

Category I errors are due to variable lag between ground command and actual shutter action on the satellite and to backlash in the gear train of the clock mechanism at the command station.

Estimates by Radio Corporation of America personnel operating the command station estimate a maximum of "something under a second" for each of these. The maximum error of two seconds is an order of magnitude smaller than other items discussed below and can therefore be neglected. Because orientation and distortion do not affect time determination here, this category contains no significant error in camera position, i.e. errors no larger than ± 1 mile in height and ± 1 mile in position of ssp.

Category II errors consist of the insignificant contribution of Category I and in addition the errors in time determination made from horizon angle measurements. These in turn are caused by the experimental error in measuring the image and any error that may exist in the value used for the spin axis orientation.

The standard deviation of the nadir angle due to uncertainty in right ascension and declination of the spin axis is shown to be 3.5° in the following section under the heading of "Effect of Spin Axis Orientation". Thus $\sigma_o = 3.5^\circ$ and $\sigma_o^2 = 12.7$. In addition to the spin axis dispersion, the procedure for measuring horizon angles introduces other errors.

The method of measuring the horizon image involves adjusting enlargement size of the image to match the fiducial marks on the calibration target, or a similar technique. Thus any misjudgement in matching image sizes and any error in reading the angle from the polar target will yield an erroneous object space angle. Due to the fact that a complete sequence of nadir angles is computed in this manner, a least squares line fitted to the whole sequence minimizes any random error.

Independent operators measuring the same sequence obtained consistent results. The maximum difference on any individual measurement was something under 4° , and following the assumptions listed in the opening of this section, we will assume $4^\circ = \pm 2\sigma$. In each sequence 10 to 30 independent measurements were made. Taking 20 as an average, we can obtain the error in nadir angle represented by the line of least squares fit by

$$\sigma_{\bar{\eta}} = \frac{\sigma_{\eta}^2}{N-1} \quad (\text{for a small sample})$$

where: σ_{η}^2 = variance of the individual nadir angle measurements
 $\sigma_{\bar{\eta}}^2$ = variance of the mean
 N = number of items in the sample.

Therefore,

$$\sigma_{\bar{\eta}}^2 = \frac{(2^\circ)^2}{19} = 0.21$$

In making time determination by matching the measured nadir angles to nadir angles derived from the nomogram, experimental error in reading the graph contributes a time error. A measure of this factor was obtained by computing a few nadir angles analytically for comparison with the graphical results. The mean root square of the differences between the results for eleven cases was 0.65° . Only one difference was greater than 1.0° (viz., 1.4°). The variance due to the "graphical" error is,

$$\sigma_g^2 = .65^2 = 0.43$$

Combining the variance due to spin axis dispersion, experimental error in measuring the image and in reading the graphical values,

$$\sigma_{II}^2 = \sigma_{\bar{\eta}}^2 + \sigma_o^2 + \sigma_g^2 = 0.21 + 12.7 + 0.43 = 13.3$$

$$\sigma_{II} = \sqrt{13.3} = 3.65^\circ$$

where, σ_{II}^2 and σ_{II} are the variance and standard derivation, respectively, of the nadir angle error for Category II pictures.

The time error corresponding to a given angle error depends upon the time rate of change of that angle. During the entire operating period of TIROS I the spin axis was no more than 25° out of the orbital plane and a reasonable average for the operating period is 10° . Table II shows that this corresponds to a rate of $3.5^\circ \text{ min.}^{-1}$ for most of the pictures involved in this type of time determination. Therefore, the angle error σ_{II} corresponds to a time error $3.65/3.5 = 1.04$ minutes which in turn corresponds to an uncertainty of ~~305~~²¹⁷ n. mi. in location of the subsatellite point.

Insofar as the assumptions concerning normally distributed, independent errors are valid, this result can be interpreted to mean that in 68% of the cases where time is determined by this method, the time error will be a minute or less. The mean orbital speed of TIROS I was 3.62° of great circle arc per minute, so in 68% of the cases Category II picture principal points will be located with an error of 217 n. mi. or less.

Reference to Table IV will show the passes on which the spin axis orientation is well documented by resection data, and all such passes may be considered as part of this second category.

TABLE IV. PHOTOGRAMMETRIC ORIENTATION FIXES OF TIROS I SPIN AXIS

<u>Readout Stn & Pass No.*</u>	<u>Frame No.</u>	<u>Date 1960</u>	<u>Time GMT</u>	<u>Right Ascension</u>	<u>Declin- ation</u>	<u>Geographical area</u>
M 002-D	4	April 1	1520:45	59.4	11.9	St. Lawrence
	5		1521:25	61.5	9.4	
K 009	14	April 2	0259:05	59.7	14.9	China, Japan, USSR
	15		0258:35	57.8	16.6	
M 016	12		1258:50	61.3	14.0	Tunisia, Sicily, Spain
	13		1258:25	63.1	12.5	
	14		1258:05	64.2	9.8	
	16		1256:55	60.9	14.5	
K 031	19	April 3	1347:25	66.8	3.0	Northwest Africa
	20		1347:15	60.7	5.6	
	21		1346:45	64.7	5.8	
K 032	20		1531:25	63.3	11.5	West Africa
	21		1531:05	65.0	6.3	
	22		1530:40	66.7	3.6	
M 043	8	April 4	0940:05	62.7	7.0	Persian Gulf
	10		0939:00	61.2	10.0	
M 044	2		1119:05	62.0	7.5	Egypt, Red Sea
	4		1118:05	61.3	6.5	
	5		1117:05	61.3	7.0	
K 045	17		1253:40	61.4	7.6	Gibraltar
	18		1253:05	59.5	13.0	
K 047	16		1437:15	58.8	8.7	Canary Islands, West Africa
	17		1436:40	61.9	7.5	
M 058	8	April 5	1025:10	64.3	2.8	Eastern Mediterranean
	9		1024:40	64.2	2.9	
K 060	17		1201:35	62.8	4.2	Spain, Gibraltar
	18		1201:10	63.9	2.9	
	19		1200:30	62.0	6.4	

*Letters "M" and "K" preceding pass number refers to readout stations at Monmouth, N.J. and Kaena Point, Hawaii, respectively. The letter "D" indicates a direct picture, all others are taped pictures. Analyses are made on Camera 2 (wide angle) pictures except where noted.

TABLE IV-(Continued)

<u>Readout Stn & Pass No.</u>	<u>Frame No.</u>	<u>Date 1960</u>	<u>Time GMT</u>	<u>Right Ascension</u>	<u>Declin- ation</u>	<u>Geographical area</u>
M 072	7	April 6	0937:40	62.3	-1.5	Southern Saudi Arabia
	8		0937:10	62.5	-1.9	
M 073	12		1112:55	59.4	-0.4	Libya
	13		1112:25	59.2	-0.6	
	14		1112:10	62.6	-2.6	
K 075	7		1437:20	52.8	3.9	West Africa
	8		1436:50	58.9	-0.8	
	9		1436:25	65.0	-2.7	
M 076-D	4		1479:40	62.9	-3.2	Florida
	5		1750:00	62.1	-0.2	
M 086	3	April 7	0844:30	61.9	-2.0	Persian Gulf
	4		0844:00	62.1	-2.0	
	5		0843:35	63.1	-2.7	
M 087	13		1018:30	62.8	-2.6	Eastern Mediterranean
	14		1018:05	63.1	-2.4	
	15		1017:30	63.9	-0.7	
K 089	3		1342:30	58.7	0.7	Northwest Africa
	4		1342:05	61.5	0.6	
	5		1341:55	60.5	-1.5	
M 101	6	April 8	0931:05	64.1	-7.1	Red Sea
	8		0930:05	62.3	-6.8	
	9		0929:35	63.2	-7.6	
K 132	20	April 10	1249:05	54.7	-8.1	West Africa
	21		1248:40	54.8	-9.5	
	22		1248:10	55.8	-11.2	
M 144	8	April 11	0836:10	66.1	-14.8	Red Sea
	9		0835:30	65.9	-12.5	
	10		0835:00	63.8	-13.9	
M 158	30	April 12	0747:00	65.2	-14.7	Saudi Arabia
M 172	21	April 13	0654:30	67.1	-16.9	Southern Saudi Arabia
	22		0654:00	67.4	-17.4	
	24		0653:30	66.3	-17.7	
M 175	18		1153:50	63.2	-17.1	West Africa
	19		1153:10	60.9	-16.4	
	20		1152:35	69.8	-16.5	

TABLE IV-(Continued)

<u>Readout Stn & Pass No.</u>	<u>Frame No.</u>	<u>Date 1960</u>	<u>Time GMT</u>	<u>Right Ascension</u>	<u>Declin- ation</u>	<u>Geographical area</u>
M 189	16	April 14	1112:25	62.9	-21.4	Southwest Africa, Angola
	17		1112:05	66.9	-22.2	
	18		1111:40	70.0	-24.7	
K 207	13	April 15	1658:55	71.4	-24.2	Western South America
	14		1658:25	68.9	-24.8	
M 231	15	April 17	0839:45	77.3	-27.3	Madagascar
	16		0839:10	76.1	-26.5	
M 274	22	April 20	0744:40	78.7	-28.6	Madagascar
	23		0744:10	80.6	-28.9	
K 337	13	April 24	1601:55	88.0	-25.2	Argentina
	14		1601:10	87.3	-24.4	
M 347	25	April 25	0826:50	79.8	-23.3	South Africa
	26		0826:40	85.0	-24.4	
K 394	30	April 28	1413:00	87.1	-17.3	Southern South America
K 466	19	May 3	1332:25	96.2	2.0	South Africa
	20		1332:00	99.2	4.3	
K 480	31	May 4	1239:35	90.1	-2.9	South Africa
M 486	28		1738:50	92.7	5.7	Uruguay, southern Brazil
	29		1738:05	91.4	-2.0	
M 491	31	May 5	0654:10	93.5	4.7	Australia
K 538	4	May 8	1251:45	86.4	10.6	Persian Gulf, Red Sea
	5		1251:15	87.5	11.0	
	14		1246:45	87.3	10.1	
K 552	9	May 9	1158:45	88.0	13.3	Arabia, Somaliland
	10		1158:15	88.0	13.9	
	17		1154:50	89.0	14.3	
M 574		May 11	0005:00	94.8	22.0	South Pacific Ocean
			0008:42	93.3	24.0	
M 575			0147:36	91.6	23.4	
			0144.42	94.2	21.1	

TABLE IV-(Continued)

<u>Readout Stn & Pass No.</u>	<u>Frame No.</u>	<u>Date 1960</u>	<u>Time GMT</u>	<u>Right Ascension</u>	<u>Declin- ation</u>	<u>Geographical area</u>
588		May 11	2312:42 2317:12	93.5 92.6	24.9 26.7	South Pacific Ocean
M 589		May 12	0054:06 0056:54	92.1 90.8	24.6 27.1	
M 602	18 19		2239:35 2239:00	101.8 100.7	34.3 33.6	Baja, California
K 609	20 23	May 13	1011:55 1010:30	98.8 98.7	33.0 31.8	West Pakistan
M 616	3		2146:00	99.8	34.9	Baja, California
K 638	19 27 28	May 15	1008:00 1003:55 1003:25	104.4 102.8 100.9	39.5 38.6 38.9	Middle East, Aden, Persian Gulf
M 643	16 17		1329:45 1329:15	112.9 116.9	44.0 49.0	Libya
K 652	18 19 22	May 16	0916:25 0916:00 0914:30	105.9 109.5 106.6	40.2 41.8 42.5	Middle East
M 657	16 17 18		1238:05 1237:25 1237:00	112.2 105.0 109.2	44.9 43.1 42.2	Egypt, Libya, Tunisia
M 658-D	10 13		1912:25 1913:25	106.6 107.6	45.2 41.5	Florida, Gulf of Mexico
K 666	20 22	May 17	0825:00 0824:00	111.1 110.4	44.4 44.1	West Pakistan
M 672	14 15 16		1147:00 1146:30 1146:00	112.8 111.8 112.4	45.4 45.3 43.8	Eastern Mediterranean
M 674-D	18		2148:00	112.7	46.3	Great Lakes
K 681	20 22 23	May 18	0913:25 0912:25 0912:00	113.0 114.1 119.6	43.9 45.2 45.3	Persian Gulf
M 686-D	10		1727:01 1727:31	118.1 117.7	46.6 47.1	Cuba (Camera 1) " Florida

TABLE IV-(Continued)

<u>Readout Stn & Pass No.</u>	<u>Frame No.</u>	<u>Date 1960</u>	<u>Time GMT</u>	<u>Right Ascension</u>	<u>Declin- ation</u>	<u>Geographical area</u>
M 688	2	May 18	2049:35	115.7	45.2	South & Baja Calif
	3		2049:10	121.4	46.3	
	4		2048:40	121.4	46.3	
M 688-D	15		2055:30	122.5	49.2	Great Lakes
K 695	15	May 19	0819:25	119.8	46.5	East Africa, Red Sea
	22		0815:50	116.8	45.6	
	23		0815:30	123.2	46.5	
M 700	24		1322:55	122.2	45.9	Gibraltar, Northwest
	25		1322:30	126.8	46.8	
M 701-D	8		1817:30	122.9	45.6	Florida
K 709	17	May 20	0728:25	124.1	48.8	West Pakistan, Iran, Saudi Arabia
	18		0728:00	126.6	48.0	
M 715-D	2		1721:59	126.2	45.7	Florida, Yucatan, Cuba
M 715-D	6		1723:30	127.3	46.1	Florida
	7		1723:55	125.2	46.9	
K 724	20	May 21	0818:05	130.3	47.0	Persian Gulf
	22		0817:10	135.9	45.1	
	23		0816:25	125.8	42.4	
M 731-D	8		2000:00	133.6	45.6	Great Lakes (Camera 1)
	9		2000:30	130.7	46.1	
M 743	23	May 22	1227:30	138.3	45.8	Gibraltar
	24		1227:05	138.7	46.0	
	25		1226:40	142.7	49.1	
M 760-D	12	May 23	1957:21	137.2	42.9	Great Lakes
M 945	11	June 5	1225:50	157.8	7.6	Red Sea, Nile River
	12		1225:30	158.5	3.4	
	13		1225:00	159.5	3.8	
	23		1220:05	159.5	1.3	
M 959	22	June 6	1127:00	157.4	2.9	Eastern Mediterra- nean
	24		1126:00	156.6	2.7	
	25		1125:30	157.7	3.1	

TABLE IV-(Continued)

<u>Readout Stn & Pass No.</u>	<u>Frame No.</u>	<u>Date 1960</u>	<u>Time GMT</u>	<u>Right Ascension</u>	<u>Declin- ation</u>	<u>Geographical area</u>
M 974	16	June 7	1040:35	154.7	-0.8	Saudi Arabia
	17		1040:00	160.8	-2.3	
	19		1039:00	158.3	-0.1	
M 988	19	June 8	1130:25	157.0	-0.6	Red Sea,
	22		1128:50	155.4	4.3	Gulf of Aden
	28		1126:05	158.1	-4.4	
M 992-D	12		1941:35	156.4	-11.9	Gulf of Mexico
	14		1942:15	157.1	-3.0	
M 1006-D	3	June 9	1848:55	159.6	-8.8	Florida, Yucatan,
	4		1849:15	157.1	-8.0	Cuba

Category III pictures timed by means of the nadir angle have a larger uncertainty because the spin axis orientation is not as well documented by resection data. For example, the period from May 24 to June 4 did not produce a single picture adequate for resection and the orientation curves are interpolated for this 12-day period. The conservative nature of the spin axis motion provides considerable confidence that the interpolated sections are satisfactory, but no reliable estimate of error can be made at this writing.

A crude estimate of the uncertainty can be obtained from the correspondence between the programmed starting time of taped pictures and the starting times deduced by nadir angle measurements and the nomogram. The apparent error of starting times appears to be no greater during this period than in periods of better orientation data. Since the apparent starting time errors are based on the interpolated part of the curves, figure 2, this indicates that the interpolation is not much less accurate than other portions of the curves. A realistic error estimate might be a standard deviation of 1.5 minute, which in turn corresponds to a nadir angle uncertainty of $\pm 5.5^\circ$ for Category III ($\sigma_{III} = 5.5^\circ$) corresponding to 325 n. mi.

Effects of Distortion on Time Determination

Distortion of the image produces error in object space angles derived from image measurements. When the image is projected on the calibration target, figures 6 or 7, the system distortion (which transformed the concentric circles in object space to irregular ovals on the image) is largely compensated because object space angles can be read directly from the distorted target. This does not compensate for a horizontal or vertical stretching of the monitor pattern however. Due to electronic changes, the ratio of width to height of the image changed from time to time. Consequently when a non-square image is projected upon a "squared-up" calibration target, it is impossible to match all fiducial marks and the operator is forced to make an estimated best fit. As a result, the angles are overestimated along one axis and underestimated along the other axis.

This effect is clear when a sequences of nadir angles is plotted because the points describe a sinusoidal oscillation about the line representing the curve of nadir angle versus time, as illustrated in figure 8a. In sequences where the horizon rotates about the picture format from frame to frame so that a complete cycle of this oscillation is plotted, it is easy to fit a smooth line representing the real nadir angle curve, but where the horizon changes very little from picture to picture, or where there are only a few horizon images to measure in a sequence, this type of distortion can introduce an error of 2° to 3° .

Fortunately most sequences in TIROS I are sufficiently long to minimize this error and no additional error need be added to those already discussed in Categories II and III above. The effect has been discussed here because users of these data may have occasion to make a time determination from a short sequence and they must be aware of this possible error source.

Effect of Spin (Optical) Axis Orientation

The following paragraphs indicate the basis of the nadir angle dispersion of $\sigma_o = 3.5^\circ$ which has already been used in the discussion of Category II time errors.

The right ascension and declination curves of figure 1 represent smoothed curves fitted to the data listed in Table IV. The arduous labor that produced the curves of figure 1 is not the subject of this report. It must suffice to state that photogrammetric evidence clearly indicates a short-period oscillation of the spin axis, and this is suggested by the variability of the right ascension and declination within the same picture sequence, shown in Table IV. Part of the scatter, however, is caused by experimental error in the resection analysis. The data available at this writing are not adequate to delineate the real oscillation nor to separate the actual variability from the errors. It is therefore necessary to compute the dispersion of the data about the mean curve for use as a measure of the spin axis uncertainty. It should be borne in mind that this amounts to a pessimistic view of the orientation accuracy, because many of the resection data have proved to be very accurate. The accuracy is reflected by the fact that grids of latitude-longitude computed on the basis of that orientation have fitted all visible geography within 10 to 30 miles. The reason for using the "pessimistic" value is because the ~~nomogram~~ is computed from the smoothed values of right ascension and declination; therefore, time determination made by use of the method outlined here will reflect the fact that the mean curves of figure 1 do not fit all of the best data.

The variance of the right ascension and declination values for each sequence of pictures of Table IV were computed (relative to their own mean). The result was

$$\sigma_a^2 = 15.7 \qquad \sigma_\delta^2 = 9.67$$

where σ_a^2 = variance of the right ascension values

σ_δ^2 = variance of the declination values.

Both declination and right ascension are related to nadir angle, but it can be shown that their errors do not have maximum influence at the same time. That is, at one moment there is a one-to-one relation between declination and nadir angle, but at that moment the effect of right ascension is nil, and vice versa. For that reason a realistic uncertainty of the nadir angle is represented by the uncertainty of either the declination or right ascension, but not both. If we assume that the mean variance of the two orientation angles is a reasonable estimate of the nadir angle variance,

$$\sigma_o^2 = 12.7 \quad \text{and} \quad \sigma_o = 3.5^\circ$$

where, σ_o^2 and σ_o are respectively the variance and standard deviation of the nadir angle due to dispersion of the orientation angles. This error estimate has already been used in the discussion of Category II errors.

Summary of Section IV

The most serious mapping errors for taped pictures with no landmarks result from the uncertainty in locating the earth principal point, and this in turn is produced by the time uncertainty.

A small sample of starting time errors indicates that some taped sequences may have started as much as 5 minutes different from the programmed times so it is necessary to check starting times by photogrammetry when mapping accuracy is required. Without some landmark to provide a fix someplace in the sequence, however, the spin axis orientation is not sufficiently well known to provide time more accurately than ± 1 minute for Category II sequences and ± 1.5 minute for Category III sequences. Direct picture sequences can usually be mapped to an accuracy an order of magnitude greater. The average distance of error corresponding to 1.0 min. time error is 217 n. mi.

A Request to Users of TIROS I Data

In the course of using these TIROS I pictures some research workers will find it necessary to make careful photogrammetric analyses of frames we have not used at this writing. The results of all such analysis would be a valuable addition to the data furnished in this report, because the history of the spin axis orientation could be refined and the nomogram, figure 2, improved.

For that reason the author of this report requests all such analysis results be sent to him at this Laboratory. In the event sufficient data are received, figures 1 and 2 will be revised and made available to all users of TIROS I pictures.

ACKNOWLEDGMENTS

The material presented here was drawn directly from the work of many of the staff of the Meteorological Satellite Laboratory who have been involved in all meteorological aspects of TIROS I. The design of the basic nomogram was developed by Mr. Irwin Ruff of this Laboratory.

In particular the author acknowledges the photogrammetric work of Mr. R. C. Doolittle of the Naval Photographic Interpretation Center and the digital computer application to the photogrammetry by Mr. L. I. Miller of this Laboratory. The personnel of this Laboratory who have computed, compiled, and produced the tables, statistics, and computations presented here are too numerous to list.

The work has been supported by the National Aeronautics and Space Administration.

REFERENCES

1. Bandeen, W. R., and W. P. Manger, 1960: Angular motion of the spin axis of the TIROS I meteorological satellite due to magnetic and gravitational torques. Journal of Geophysical Research, Vol. 65, No. 9, September 1960, pp. 2992-2995.
2. Doolittle, R. C., L. I. Miller and I. S. Ruff, Geographical location of cloud features. Appendix 1, of Technical Report to National Aeronautics and Space Administration, by staff of Meteorological Satellite Laboratory, United States Weather Bureau. (to be published)
3. Glaser, Arnold H., 1960: A system for the meteorological use of satellite television observations. Chapter IV of Contributions to satellite meteorology GRD Research Notes No. 36, AFCRC-TN-60-427, Geophysical Research Directorate, Bedford, Massachusetts.
4. Hubert, L. F., 1960: Analysis of project HUGO test firing December 5, 1958, Meteorological Satellite Laboratory, Report No. 2 to National Aeronautics and Space Administration. Washington, D. C.
5. Staff members, Radio Corporation of America, 1960. Sensor alignment and calibration data for TIROS I, Vehicle D-3. (Confidential). Astro-Electronic Products Division, Princeton, New Jersey.

APPENDIX I

TRANSFORMATION EQUATIONS USED FOR NOMOGRAM CONSTRUCTION

The coordinates of a transverse mercator map projection have been used for the basic nomogram discussed in Section II. This map projection is computed for a tangent cylinder which is tangent to the earth at some great circle other than the equator. For this particular application the map is "projected" onto a cylinder which is tangent to the earth along a great circle inclined 48.4° to the equatorial plane -- equivalent to the orbit of TIROS I.

While the nomogram represents the map of the celestial sphere, it is more exactly a "relative celestial sphere" because the origin is not fixed at a constant right ascension. Due to the fact that the orbital plane rotates in space, the nomogram is constructed with the origin fixed at the right ascension of the ascending node for any pass under consideration. For these reasons the equations are expressed in terms of latitude and longitude instead of declination and right ascension, and should be visualized as the latitude and longitude corresponding to the declination and right ascension at some given instant.

The resulting map is essentially a rectilinear coordinate system because within 25° of the tangent circle the mercator map projection represents degrees of latitude and degrees of longitude with almost equal length increments. The abscissa of the graph represents 2π , one complete pass of the satellite in the celestial sphere, which is labeled in terms of time, a total of 99.2 minutes. The ordinate corresponds to "latitude" on the transverse mercator projection.

The following equations transform any point defined in terms of standard geodetic coordinates of latitude and longitude to a "latitude" and "longitude" of the transverse mercator map..

Define longitude λ' and λ as the points of intersection of the transverse mercator tangency circle with the equator. For this application λ' is taken as the longitude of the ascending node of some particular pass of TIROS I.

Let "i" be the angle between the plane of the inclined transverse tangency circle and the equatorial plane; thus in this application "i" is the inclination of the TIROS I orbit. The longitudes of greatest departure of the transverse mercator tangent circle from the equator are hence $\pm i$ at longitudes $\lambda' + 90^\circ$ and $\lambda' + 270^\circ$ respectively, where longitude is measured from 0 to 360° , positive eastward.

The central meridian $\lambda = 0$ which defines the common origin of the spherical coordinates of the standard mercator and transverse mercator maps is taken at $\lambda' + 90$ because at this longitude the meridians of both the standard mercator and the transverse mercator are colinear and contain the north pole of the earth and the "latitude" of 90° referred to the transverse mercator projection.

The spherical triangles involved in this transformation are shown in figure 1 and the spherical trigonometric equations are:

$$\cos \phi_{tm} = \cos i \cos \phi_e - \sin i \sin \phi_e \cos \Delta\lambda_e$$

$$\sin \Delta\lambda_{tm} = \frac{\sin \phi_e \sin \Delta\lambda_e}{\sin \phi_{tm}}$$

where

$i = 48.4^\circ =$ inclination of the orbital plane

$P_e =$ north pole on earth, where latitude is 90°

$P_{tm} =$ "north pole" of the transverse mercator map where "latitude" is 90° , referred to transverse coordinates.

$\phi_e =$ colatitude of the point to be transformed, expressed in standard geodetic coordinates.

$\phi_{tm} =$ colatitude of the point after transformation, expressed in "latitude" of the transverse mercator map.

$$\Delta\lambda_e = (\lambda' + 90) - \lambda_p$$

$\lambda' =$ longitude of intersection, in this case longitude of the ascending node, as discussed above.

$\lambda_p =$ longitude of the point being transformed, expressed in standard geodetic coordinates.

$\Delta\lambda_{tm} =$ increment of longitude of the transformed point measured from the central meridian (discussed above) expressed in terms of transverse mercator coordinates.

The nomogram was constructed by computing the location of the Spin Axis Point for 1200 GMT of each day, April 1 through June 15, 1960. In the use of the nomogram the assumption is made that straight lines laid off between various time-positions along the orbit (abscissa) and the SAP for any specific time represent great circle arcs. Actually, such straight lines are rhumb lines, but because all of the SAP positions are no farther than 25° from the orbital plane, the approximation is a very good one.

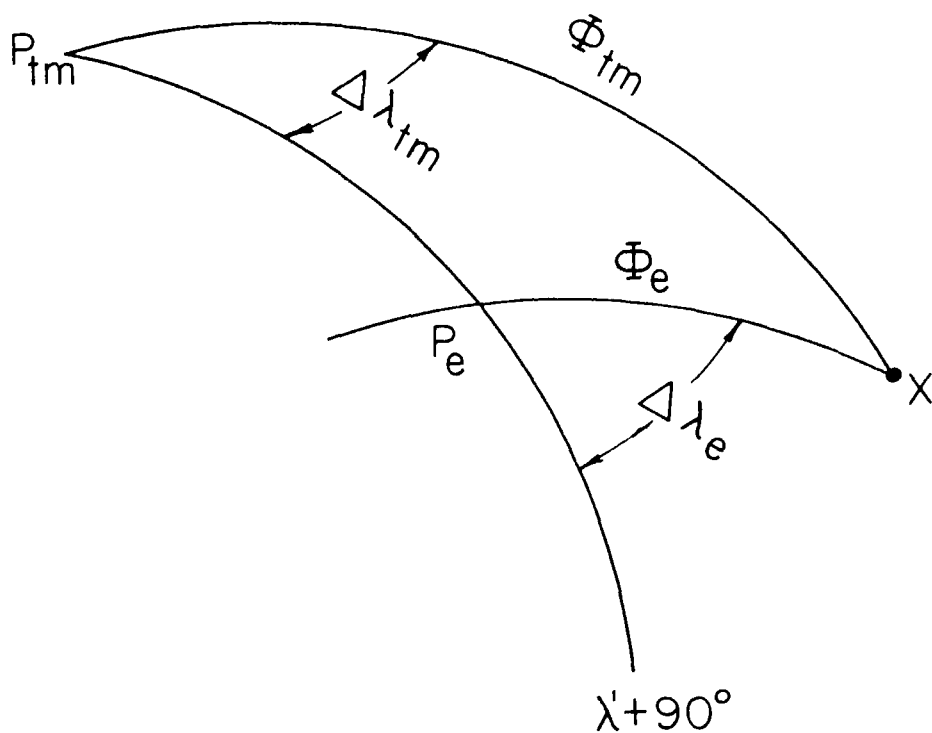


Figure 1. Spherical triangles involved in transformation of point "X" defined in standard geodetic coordinates to a transverse Mercator map projection. Symbols defined in Appendix I.

APPENDIX II

TIROS I - APPROXIMATED ORBIT AND ASCENDING NODES

The orbit of TIROS I was so slightly elliptical that it may be considered circular for some purposes. Where the subsatellite point position is required for purposes of specifying the camera location, it is frequently adequate to consider the velocity of the satellite to be constant and derive subsatellite positions by computing distances from the ascending node of that particular pass. Tables A and B are presented for that purpose.

Table A is a listing of all ascending node data for TIROS I; Table B shows the subsatellite point for each minute past the ascending node in terms of latitude and longitude on a rotating earth (which accounts for one complete pass encompassing only 334.9° of longitude). Auxiliary columns list the minute increments of latitude and longitude for convenience in interpolating intermediate positions.

Inclination of TIROS I orbit was 48.4° but combination of the perturbation produced by the equatorial bulge and the difference between geocentric and geodetic latitude resulted in the satellite reaching extreme latitudes of $\pm 48.8^\circ$. In compiling Table B, the circular orbit computed about a spherical earth has been adjusted to include that effect, so the latitudes at 24.8 and 74.4 minutes are listed $+48.8^\circ$ (North) and -48.8° (South) respectively.

The maximum error in ssp position that can result from using Table B is about 40 n. mi. and this occurs near the central part of the period (because the error must vanish at either end). The maximum error does not occur on every pass, of course.

An example is discussed here to illustrate application of these tables, using pass 116, April 9, 1960, which is the picture sequence discussed in the problem of Section II.

PROBLEM: Obtain the latitude and longitude of the subsatellite point at 38.7 min. after the ascending node of pass 116, and the Greenwich Mean Time at that position.

Step 1. From Table B obtain the latitude and longitude corresponding to 39.0 minutes and the appropriate increments. Interpolate linearly.

EXAMPLE:

$$\begin{array}{lll} 39 \text{ min.} & \phi = +28^\circ & \Delta \phi = 2.3^\circ \\ & \lambda = 139.2 & \Delta \lambda = 2.9 \end{array}$$

$$\begin{array}{ll} 38.7 \text{ min.} & \phi = 28 + 0.3 \times 2.3 = 28.7^\circ \\ & \lambda = 139.2 - 0.3 \times 2.9 = 138.3^\circ \end{array}$$

This result means that the ssp at 38.7 min. after the A. N. of pass 116 is 28.7 north of the ascending node (which is at 0° by definition) and is 138.3° of longitude east of the ascending node of pass 116. Notice that $0 \leq \lambda \leq 334.9^\circ$ and is always measured eastward.

Step 2. From Table A obtain the ascending node data for pass 116, and add the appropriate quantities from Step 1.

EXAMPLE:

For pass 116:

The A. N. longitude was 146.6°W at 1116.9 or 11:16:54 GMT

$$146.6 - 138.3 = 8.3 \text{ or } 8.3^\circ\text{W}$$

$$1116.9 + 38.7 \text{ (min)} = 11:55.6 \text{ or } 11:55:36$$

Therefore, the subsatellite point at 11:55:36 GMT, April 9, 1960, was located at 28.7°N, 8.3°W.

TABLE A. TIROS I-ASCENDING NODES-TIME AND LONGITUDE
 Time: GMT in hours, minutes and tenths
 Longitude: West and East in degrees and tenths

<u>Pass Number</u>	<u>Time</u>	<u>Longitude</u>	<u>Date</u> <u>1960</u>	<u>Pass Number</u>	<u>Time</u>	<u>Longitude</u>	<u>Date</u> <u>1960</u>
1	1313.3	131.6 W	1 Apr	40	0540.6	33.3 W	4 Apr
2	1452.5	156.7 W		41	0719.8	58.5	
3	1631.6	178.1 E		42	0858.9	83.7	
4	1810.8	152.9		43	1038.1	108.9	
5	1950.0	127.8		44	1217.3	134.0	
6	2129.1	102.6		45	1356.1	159.2 W	
7	2308.3	77.4		46	1535.6	175.6 E	
8	0047.4	52.2	2 Apr	47	1714.8	150.4	
9	0226.6	27.0		48	1853.9	125.3	
10	0405.8	1.9 E		49	2033.1	100.1	
11	0545.0	23.3 W		50	2212.2	74.9	
12	0724.1	48.5		51	2351.4	49.8	
13	0903.3	73.6		52	0130.6	24.6 E	5 Apr
14	1042.4	98.2		53	0309.7	.6 W	
15	1221.6	124.0		54	0448.9	25.8	
16	1400.8	149.2		55	0628.0	51.0	
17	1539.9	174.3 W		56	0807.2	76.1	
18	1719.1	160.5 E		57	0946.4	101.3	
19	1858.2	135.3		58	1125.5	126.5	
20	2037.4	110.1		59	1304.4	151.6	
21	2216.6	85.0		60	1443.3	176.8 W	
22	2355.7	59.8		61	1623.0	158.0 E	
23	0134.9	34.6	3 Apr	62	1802.2	132.8	
24	0314.0	9.4 E		63	1941.3	107.6	
25	0453.2	15.7 W		64	2120.5	82.5	
26	0632.4	40.9		65	2259.6	57.3	
27	0811.4	66.1		66	0038.8	32.1	6 Apr
28	0950.7	91.2		67	0218.0	7.0 E	
29	1129.8	116.4		68	0357.1	18.2 W	
30	1309.0	141.6		69	0536.3	43.4	
31	1448.0	166.8 W		70	0715.4	68.6	
32	1627.2	168.0 E		71	0854.6	93.7	
33	1806.3	142.9		72	1033.8	118.9	
34	1945.6	117.7		73	1212.9	144.1	
35	2124.8	92.5		74	1352.1	169.3 W	
36	2304.0	67.4		75	1530.3	165.6 E	
37	0043.1	42.2	4 Apr	76	1710.4	140.4	
38	0222.3	17.0 E		77	1849.6	115.2	
39	0401.4	8.2 W		78	2027.8	90.0	

Table A - (Continued)

<u>Pass</u> <u>Number</u>	<u>Time</u>	<u>Longitude</u>	<u>Date</u> <u>1960</u>	<u>Number</u>	<u>Time</u>	<u>Longitude</u>	<u>Date</u> <u>1960</u>
79	2207.9	64.9 E	6 Apr	126	0348.5	38.3 W	10 Apr
80	2347.1	39.7		127	0527.6	63.5	
81	0126.2	14.5 E	7 Apr	128	0706.8	88.7	
82	0305.4	10.6 W		129	0846.0	113.8	
83	0444.6	35.8		130	1025.1	139.0	
84	0623.7	61.0		131	1204.3	164.2 W	
85	0802.9	86.2		132	1343.4	170.6 E	
86	0942.0	111.4		133	1522.6	145.5	
87	1121.2	136.5		134	1701.8	120.3	
88	1300.4	161.7 W		135	1840.9	95.1	
89	1439.5	173.1 E		136	2020.1	69.9	
90	1618.7	148.0		137	2159.2	44.8	
91	1757.8	122.7		138	2338.4	19.6 E	
92	1937.0	97.6		139	0117.6	5.6 W	
93	2116.2	72.4		140	0256.7	30.8	
94	2255.3	47.2		141	0435.9	55.9	
95	0034.5	22.1 E	8 Apr	142	0615.0	81.1	
96	0213.6	3.1 W		143	0754.2	106.3	
97	0352.8	28.3		144	0933.4	131.4	
98	0532.0	53.4		145	1112.5	156.6 W	
99	0711.1	78.6		146	1251.7	178.2 E	
100	0850.3	103.8		147	1430.9	153.0	
101	1029.4	129.0		148	1610.0	127.8	
102	1208.6	154.1		149	1749.2	102.7	
103	1347.8	179.3 W		150	1928.3	77.5	
104	1526.9	155.5 E		151	2107.5	52.3	
105	1706.1	130.3		152	2246.7	27.2	
106	1845.2	105.2		153	0025.8	02.0 E	
107	2024.4	80.0		154	0205.0	23.2 W	
108	2202.6	54.8		155	0344.2	48.4	
109	2342.7	29.6		156	0523.3	73.5	
110	0121.9	04.5 E		9 Apr	157	0702.5	
111	0301.1	20.7 W	158		0841.6	123.9	
112	0440.2	45.9		159	1020.8	149.1	
113	0619.4	71.0		160	1200.0	174.2 W	
114	0758.6	96.2		161	1339.1	160.6 E	
115	0937.7	121.4		162	1518.3	135.4	
116	1116.9	146.6		163	1657.4	110.2	
117	1256.0	171.8 W		164	1836.6	85.1	
118	1435.2	163.1 E		165	2015.8	59.9	
119	1614.4	137.9		166	2154.9	34.7	
120	1753.5	112.7		167	2334.1	9.6 E	
121	1932.7	87.6		168	0113.2	15.6 W	
122	2111.8	62.4		169	0252.4	40.8	
123	2251.0	37.2		170	0431.6	66.0	
124	0030.2	12.0 E	10 Apr	171	0610.7	91.2	
125	0209.3	13.1 W		172	0749.9	116.3	

Table A - (Continued)

<u>Pass Number</u>	<u>Time</u>	<u>Longitude</u>	<u>Date 1960</u>	<u>Pass Number</u>	<u>Time</u>	<u>Longitude</u>	<u>Date 1960</u>
173	0929.0	141.5 W	13 Apr	220	1509.6	115.3 E	16 Apr
174	1108.2	166.7 W		221	1648.8	90.1	
175	1247.4	168.2 E		222	1827.9	65.0	
176	1426.5	143.0		223	2007.1	39.8	
177	1605.7	117.8		224	2146.2	14.6 E	
178	1744.8	92.6		225	2325.4	10.6 W	
179	1924.0	67.4		226	0104.6	35.7	17 Apr
180	2103.2	42.3		227	0243.7	60.9	
181	2242.3	17.1 E		228	0422.9	86.1	
182	0021.5	8.1 W	14 Apr	229	0602.1	111.2	
183	0200.6	33.2		230	0741.2	136.4	
184	0339.8	58.4		231	0920.4	161.6 W	
185	0519.0	83.6		232	1059.6	173.2 E	
186	0658.1	108.8		233	1238.7	148.0	
187	0837.3	133.9		234	1417.9	122.9	
188	1016.5	159.1 W		235	1557.0	97.7	
189	1155.6	175.7 E		236	1736.2	72.5	
190	1334.8	150.5		237	1915.4	47.4	
191	1514.0	125.4		238	2054.5	22.2 E	
192	1653.1	100.2		239	2233.7	3.0 W	
193	1832.3	75.0		240	0012.8	28.2	18 Apr
194	2011.4	49.8		241	0152.0	53.3	
195	2150.6	24.7 E		242	0331.2	78.5	
196	2329.8	0.5 W		243	0510.3	103.7	
197	0108.9	25.7	15 Apr	244	0649.5	128.9	
198	0248.1	50.8		245	0828.6	154.0	
199	0427.2	76.0		246	1007.8	179.2 W	
200	0606.4	101.2		247	1147.0	155.6 E	
201	0745.6	126.4		248	1326.0	130.7	
202	0924.7	151.6		249	1505.2	105.6	
203	1103.9	176.7 W		250	1644.3	80.4	
204	1243.0	158.1 E		251	1823.5	55.2	
205	1422.2	132.9		252	2002.6	30.0	
206	1601.4	107.8		253	2141.8	4.9 E	
207	1740.5	82.6		254	2320.9	20.3 W	
208	1919.7	57.4		255	0100.1	45.5	19 Apr
209	2058.8	32.2		256	0239.2	70.6	
210	2238.0	7.0 E		257	0418.4	95.8	
211	0017.2	18.1 W	16 Apr	258	0557.6	12.0	
212	0156.3	43.3		259	0736.7	146.2	
213	0335.5	68.5		260	0915.9	171.4 W	
214	0514.6	93.6		261	1055.0	163.5 E	
215	0653.8	118.8		262	1234.2	138.3	
216	0833.0	144.0		263	1413.4	113.1	
217	1012.1	169.2 W		264	1552.5	88.0	
218	1151.3	165.7 E		265	1731.7	62.8	
219	1330.4	140.5		266	1910.8	37.6	

Table A - (Continued)

<u>Pass Number</u>	<u>Time</u>	<u>Longitude</u>	<u>Date 1960</u>	<u>Pass Number</u>	<u>Time</u>	<u>Longitude</u>	<u>Date 1960</u>
267	2050.0	12.4 E	19 Apr	313	0051.4	65.3	23 Apr
268	2229.2	12.7 W		314	0230.5	90.5	
269	0008.3	37.9	20 Apr	315	0409.7	115.6	
270	0147.5	63.1		316	0548.8	140.8	
271	0326.6	88.2		317	0728.0	166.0 W	
272	0505.8	113.4		318	0907.2	168.8 E	
273	0645.0	138.6		319	1046.3	143.6	
274	0824.1	163.8 W		320	1225.5	118.5	
275	1003.3	171.0 E		321	1404.6	93.3	
276	1142.4	145.9		322	1543.8	68.1	
277	1321.6	120.7		323	1723.0	43.0	
278	1500.8	95.5		324	1902.1	17.8 E	
279	1639.9	70.4		325	2041.3	7.4 W	
280	1819.1	45.2		326	2220.4	32.6	
281	1958.2	20.0 E		327	2359.6	57.7	
282	2137.4	5.2 W		328	0138.8	82.9	24 Apr
283	2316.6	30.3		329	0317.9	108.1	
284	0055.7	55.5	21 Apr	330	0457.1	133.2	
285	0234.9	80.7		331	0636.2	158.4 W	
286	0414.0	105.8		332	0815.4	176.4 E	
287	0553.2	131.0		333	0954.6	151.2	
288	0732.3	156.2 W		334	1133.7	126.0	
289	0911.5	178.6 E		335	1312.9	100.9	
290	1050.6	153.4		336	1452.0	75.7	
291	1229.8	128.3		337	1631.2	50.5	
292	1409.0	103.1		338	1810.4	25.4	
293	1548.1	77.9		339	1949.5	0.2 E	
294	1727.3	52.8		340	2128.7	25.0 W	
295	1906.4	27.6		341	2307.8	50.2	
296	2045.6	2.4 E		342	0047.0	75.3	25 Apr
297	2224.8	22.8 W		343	0226.1	100.5	
298	0003.9	47.9	22 Apr	344	0405.3	125.7	
299	0143.1	73.1		345	0544.4	150.8	
300	0322.3	98.1		346	0723.6	176.0 W	
301	0501.5	123.2		347	0902.8	158.8 E	
302	0640.6	148.4		348	1041.9	133.6	
303	0819.8	173.6 W		349	1221.1	108.4	
304	0959.0	161.2 E		350	1400.2	83.3	
305	1138.1	136.1		351	1539.4	58.1	
306	1317.3	110.9		352	1718.6	32.9	
307	1456.4	85.7		353	1857.7	7.8 E	
308	1635.6	60.6		354	2036.9	17.4 W	
309	1814.8	35.4		355	2216.0	42.6	
310	1953.9	10.2 E		356	2355.2	67.8	
311	2133.1	15.0 W		357	0134.4	92.9	26 Apr
312	2312.2	40.1		358	0313.5	118.1	

Table A - (Continued)

<u>Pass Number</u>	<u>Time</u>	<u>Longitude</u>	<u>Date 1960</u>	<u>Pass Number</u>	<u>Time</u>	<u>Longitude</u>	<u>Date 1960</u>
359	0452.7	143.3 W	26 Apr	406	1033.2	114.1 E	29 Apr
360	0631.8	168.4 W		407	1212.4	88.9	
361	0811.0	166.4 E		408	1351.6	63.7	
362	0950.2	141.2		409	1530.7	38.6	
363	1129.3	116.0		410	1709.9	13.4 E	
364	1308.5	90.8		411	1849.0	11.8 W	
365	1447.6	65.7		412	2028.2	37.0	
366	1626.8	40.5		413	2207.4	62.1	
367	1805.9	15.3 E		414	2346.5	87.3	
368	1945.1	9.8 W		415	0125.7	112.5	30 Apr
369	2124.2	35.0		416	0304.8	137.6	
370	2303.4	60.2		417	0444.0	162.8 W	
371	0042.6	85.4	27 Apr	418	0623.2	172.0 E	
372	0221.7	110.5			419	0802.3	146.8
373	0400.9	135.7		420	0941.5	121.7	
374	0540.0	160.9 W		421	1120.6	96.5	
375	0719.2	174.0 E		422	1259.8	71.3	
376	0858.4	148.8		423	1439.0	46.2	
377	1037.5	123.6		424	1618.1	21.0 E	
378	1216.7	98.4		425	1757.3	4.2 W	
379	1355.8	73.2		426	1936.4	29.4	
380	1535.0	48.1		427	2115.6	54.5	
381	1714.2	22.9 E		428	2254.8	79.7	
382	1853.3	2.3 W		429	0033.9	104.9	1 May
383	2032.5	27.4		430	0213.1	130.0	
384	2211.6	52.6		431	0352.2	155.2 W	
385	2350.8	77.8		432	0531.4	179.6 E	
386	0130.0	103.0	28 Apr	433	0710.6	154.4	
387	0309.1	128.1			434	0849.7	129.3
388	0448.3	153.3		435	1028.9	104.1	
389	0627.4	178.5 W		436	1208.0	79.0	
390	0806.6	156.4 E		437	1347.2	53.8	
391	0945.7	131.2		438	1526.4	28.6	
392	1125.0	106.4		439	1705.5	03.4 E	
393	1304.2	81.3		440	1844.7	21.7 W	
394	1443.4	56.1		441	2023.8	46.9	
395	1622.5	31.0		442	2203.0	72.1	
396	1801.7	5.8 E		443	2342.2	97.2	
397	1940.8	19.4 W		444	0121.3	122.4	2 May
398	2120.0	44.6		445	0300.5	147.6	
399	2259.1	69.7		446	0439.6	172.8 W	
400	0038.3	94.9	29 Apr	447	0618.8	162.1 E	
401	0217.5	120.1			448	0757.9	136.9
402	0356.6	145.2		449	0937.1	111.7	
403	0535.8	170.4 W		450	1116.3	86.6	
404	0714.9	164.4 E		451	1255.4	61.4	
405	0854.1	139.2		452	1434.6	36.2	

Table A - (Continued)

<u>Pass Number</u>	<u>Time</u>	<u>Longitude</u>	<u>Date 1960</u>	<u>Pass Number</u>	<u>Time</u>	<u>Longitude</u>	<u>Date 1960</u>
453	1613.7	11.0 E	2 May	500	2150.1	92.0 W	5 May
454	1752.9	14.1 W		501	2333.3	117.1 W	6 May
455	1932.0	39.3	3 May	502	0112.4	142.3	
456	2111.2	64.5		503	0251.6	167.5 W	
457	2250.4	89.6		504	0430.8	167.4 E	
458	0029.5	114.8		505	0609.9	142.2	
459	0208.7	140.0		506	0749.1	117.0	
460	0347.8	165.2 W		507	0928.2	91.8	
461	0527.0	169.7 E		508	1107.4	66.7	
462	0706.2	144.5		509	1246.6	41.5	
463	0845.3	119.3		510	1425.7	16.3 E	
464	1024.5	94.2		511	1604.8	8.8 W	
465	1203.6	69.0	512	1744.0	34.0	8 May	
466	1342.8	43.8	513	1923.2	59.2		
467	1522.0	18.6 E	514	2102.3	84.4		
468	1701.1	6.5 W	515	2241.5	109.5		
469	1840.3	31.7	516	0020.6	134.7		
470	2019.4	56.9	517	0159.8	159.9 W		
471	2158.6	82.0	518	0339.0	175.0 E		
472	2337.8	107.2	519	0518.1	149.8		
473	0116.9	132.4	520	0657.3	124.6		
474	0256.1	157.6 W	521	0836.4	99.4		
475	0435.2	177.3 E	522	1015.6	74.3	9 May	
476	0614.4	152.1	523	1154.8	49.1		
477	0753.6	127.0	524	1333.9	24.0 E		
478	0932.7	101.8	525	1513.1	1.2 W		
479	1111.9	76.6	526	1652.2	26.4		
480	1251.0	51.4	527	1831.4	51.6		
481	1430.2	26.3	528	2010.5	76.7		
482	1609.4	1.1 E	529	2149.7	101.9		
483	1748.5	24.1 W	530	2328.8	127.1		
484	1927.7	49.2	531	0108.0	152.2		
485	2106.8	74.4	532	0247.2	177.4 W	9 May	
486	2246.0	99.6	533	0426.3	157.4 E		
487	0025.2	124.8	534	0605.5	132.2		
488	0204.3	149.9	535	0744.6	107.1		
489	0343.5	175.1 W	536	0923.8	81.9		
490	0522.6	159.7 E	537	1103.0	56.7		
491	0701.8	134.6	538	1242.1	31.6		
492	0841.0	109.4	539	1421.3	6.4 E		
493	1020.1	84.2	540	1600.4	18.8 W		
494	1159.2	59.1	541	1739.6	44.0		
495	1338.3	33.9	542	1918.8	69.1	9 May	
496	1517.5	8.7 E	543	2057.9	94.3		
497	1656.6	16.4 W	544	2237.1	119.5		
498	1835.8	41.6	545	0016.2	144.6		
499	0522.6	159.7 E	546	0155.4	169.8 W		

Table A - (Continued)

<u>Pass Number</u>	<u>Time</u>	<u>Longitude</u>	<u>Date 1960</u>	<u>Pass Number</u>	<u>Time</u>	<u>Longitude</u>	<u>Date 1960</u>
547	0334.5	165.0 E	9 May	594	0914.9	62.0 E	12 May
548	0513.7	132.8		595	1054.1	36.8	
549	0652.8	114.7		596	1233.2	11.7 E	
550	0832.0	89.5		597	1412.4	13.5 W	
551	1011.2	64.4		598	1551.6	38.6	
552	1150.3	39.2		599	1730.7	63.8	
553	1329.5	14.0 E		600	1909.9	89.0	
554	1508.6	11.2 W		601	2049.0	114.2	
555	1647.8	36.3		602	2228.2	139.3	
556	1827.0	61.5		603	0007.4	164.5 W	
557	2006.1	86.7	604	0146.5	170.3 E		
558	2145.3	111.8	605	0325.7	145.2		
559	2324.4	137.0	606	0504.8	120.0		
560	0103.6	162.2 W	10 May	607	0644.0	94.8	
561	0242.8	172.6 E		608	0823.1	69.6	
562	0421.9	147.5		609	1002.3	44.5	
563	0601.0	122.3		610	1141.5	19.3 E	
564	0740.2	97.1		611	1320.6	5.9 W	
565	0919.4	72.0		612	1459.8	31.0	
566	1058.5	46.8		613	1639.0	56.2	
567	1237.7	21.6 E		614	1818.1	81.4	
568	1416.8	3.6 W		615	1957.3	106.6	
569	1656.0	28.7		616	2136.4	131.7	
570	1735.2	53.9	617	2315.6	156.9 W	14 May	
571	1914.3	79.1	618	0054.8	177.9 E		
572	2053.5	104.2	619	0233.9	152.8		
573	2232.6	129.4	620	0413.1	127.6		
574	0011.8	154.6	11 May	621	0552.2		102.4
575	0151.0	179.7 W		622	0731.4		77.2
576	0330.1	155.1 E		623	0910.5		52.1
577	0509.3	129.9		624	1049.7		26.9
578	0648.4	104.8		625	1228.8		1.7 E
579	0827.6	79.6		626	1408.0		23.4 W
580	1006.7	54.4		627	1547.2	48.6	
581	1145.9	29.2		628	1726.3	73.8	
582	1325.0	4.1 E		629	1905.5	98.9	
583	1504.2	21.1 W		630	2044.6	124.1	
584	1643.4	46.3	631	2223.8	149.3	15 May	
585	1822.5	71.4	632	0003.0	174.4 W		
586	2001.7	96.6	633	0142.1	160.4 E		
587	2140.8	121.8	634	0321.3	135.2		
588	2320.0	147.0	635	0500.4	110.0		
589	0059.2	172.1 W	12 May	636	0639.6		84.9
590	0238.3	162.7 E		637	0818.7		59.7
591	0417.5	137.5		638	0957.9		34.5
592	0556.6	112.4		639	1137.0		9.4 E
593	0735.8	87.2		640	1316.2		15.8 W

Table A - (Continued)

<u>Pass Number</u>	<u>Time</u>	<u>Longitude</u>	<u>Date 1960</u>	<u>Pass Number</u>	<u>Time</u>	<u>Longitude</u>	<u>Date 1960</u>
641	1455.4	41.0 W	15 May	688	2035.8	144.0 W	18 May
642	1634.5	66.2		689	2214.9	169.2 W	
643	1813.7	91.3		690	2354.1	165.7 E	
644	1952.8	116.5		691	0133.2	140.5	19 May
645	2132.0	141.7		692	0312.4	115.3	
646	2311.2	166.8 W		693	0451.5	90.2	
647	0050.3	168.0 E	16 May	694	0630.7	65.0	
648	0229.5	142.8		695	0809.8	39.8	
649	0408.6	117.6		696	0949.0	14.6 E	
650	0547.8	92.5		697	1128.2	10.5 W	
651	0726.9	67.3		698	1307.3	35.7	
652	0906.1	42.2		699	1446.5	60.8	
653	1045.2	17.0 E		700	1625.6	86.0	
654	1224.4	8.2 W		701	1804.8	111.2	
655	1403.6	33.4		702	1944.0	136.4	
656	1542.7	58.5		703	2123.1	161.5 W	
657	1721.9	83.7		704	2302.2	173.3 E	
658	1901.0	108.9		705	0041.4	148.1	20 May
659	2040.2	134.0		706	0220.6	123.0	
660	2219.4	159.2 W		707	0359.7	97.8	
661	2358.5	175.6 E		708	0538.9	72.6	
662	0137.7	150.4	17 May	709	0718.0	47.4	
663	0316.8	125.3		710	0857.2	22.3 E	
664	0456.0	100.1		711	1036.4	2.9 W	
665	0635.1	74.9		712	1215.6	28.1	
666	0814.3	49.8		713	1354.8	53.3	
667	0953.4	24.6 E		714	1533.9	78.4	
668	1132.6	0.6 W		715	1713.1	103.6	
669	1311.8	25.8		716	1852.2	128.8	
670	1450.9	50.9		717	2031.4	154.0	
671	1630.1	76.1		718	2210.6	179.1 W	
672	1809.2	101.3		719	2349.7	155.7 E	
673	1948.4	126.4		720	0128.9	130.6	21 May
674	2127.6	151.6		721	0308.0	105.4	
675	2306.7	176.8 W		722	0447.2	80.2	
676	0045.9	158.0 E	18 May	723	0626.4	55.0	
677	0225.0	132.9		724	0805.5	29.9	
678	0404.2	107.7		725	0944.7	4.7 E	
679	0543.3	82.6		726	1123.8	20.5 W	
680	0722.5	57.4		727	1303.0	45.6	
681	0901.6	32.2		728	1442.1	70.8	
682	1040.8	7.0 E		729	1621.3	96.0	
683	1220.0	18.1 W		730	1800.4	121.2	
684	1359.1	43.3		731	1939.6	146.3	
685	1538.3	68.5		732	2118.8	171.5 W	
686	1717.4	93.6		733	2257.9	163.3 E	
687	1856.6	118.8		734	0037.1	138.2	22 May

Table A - (Continued)

<u>Pass Number</u>	<u>Time</u>	<u>Longitude</u>	<u>Date 1960</u>	<u>Pass Number</u>	<u>Time</u>	<u>Longitude</u>	<u>Date 1960</u>	
735	0216.2	113.0 E	22 May	782	0756.6	10.0 E	25 May	
736	0355.4	87.8		783	0935.8	15.2 W		
737	0534.6	62.6		784	1114.9	40.4		
738	0713.7	37.5		785	1254.1	65.5		
739	0852.9	12.3 E		786	1433.2	90.7		
740	1032.0	12.8 W		787	1612.4	115.8		
741	1211.2	38.0		788	1751.6	141.0		
742	1350.3	63.2		789	1930.7	166.2 W		
743	1529.5	88.4		790	2109.9	168.6 E		
744	1708.6	113.5		791	2249.0	143.5		
745	1847.8	138.7		792	0028.2	118.3		26 May
746	2027.0	163.9 W		793	0207.3	93.1		
747	2206.1	171.0 E		794	0346.5	68.0		
748	2345.3	145.8		795	0525.6	42.8		
749	0124.4	120.6	23 May	796	0704.8	17.6 E		
750	0303.6	95.4		797	0844.0	7.6 W		
751	0442.8	70.3		798	1023.1	32.7		
752	0621.9	45.1		799	1202.3	57.9		
753	0801.1	19.9 E		800	1341.4	83.1		
754	0940.2	5.2 W		801	1520.6	108.2		
755	1119.4	30.4		802	1659.8	133.4		
756	1258.5	55.6		803	1838.9	158.6 W		
757	1437.7	80.8		804	2018.1	176.2 E		
758	1616.8	105.9		805	2157.2	151.1		
759	1756.0	131.1		806	2336.4	125.9		
760	1935.2	156.3 W		807	0115.5	100.7	27 May	
761	2114.3	178.6 E		808	0254.7	75.6		
762	2253.5	153.4		809	0433.8	50.4		
763	0032.6	128.2	24 May	810	0613.0	25.2		
764	0211.8	103.0		811	0752.2	0.1 E		
765	0351.0	77.9		812	0931.3	25.1 W		
766	0530.1	52.7		813	1110.5	50.3		
767	0709.3	27.6		814	1249.7	75.5		
768	0848.4	2.4 E		815	1428.8	100.6		
769	1027.6	22.8 W		816	1608.0	125.8		
770	1206.7	48.0		817	1747.1	151.0		
771	1345.9	73.1		818	1926.3	176.1 W		
772	1525.0	98.3		819	2105.4	158.7 E		
773	1704.2	123.5		820	2244.6	133.5		
774	1843.4	148.6		821	0023.8	108.4	28 May	
775	2022.5	173.8 W		822	0202.9	83.2		
776	2201.7	161.0 E		823	0342.1	74.0		
777	2340.8	135.8	824	0521.2	32.8			
778	0120.0	110.7	25 May	825	0700.4	7.7 E		
779	0259.2	85.5		826	0839.6	17.5 W		
780	0438.3	60.3		827	1018.7	42.7		
781	0617.4	35.2		828	1157.8	67.8		

Table A - (Continued)

<u>Pass</u> <u>Number</u>	<u>Time</u>	<u>Longitude</u>	<u>Date</u> <u>1960</u>	<u>Pass</u> <u>Number</u>	<u>Time</u>	<u>Longitude</u>	<u>Date</u> <u>1960</u>
829	1337.0	93.0 W	28 May	876	1917.4	164.0 E	31 May
830	1516.2	118.2		877	2056.6	138.8	
831	1655.3	143.4	29 May	878	2235.7	113.6	1 Jun
832	1834.5	168.5 W		879	0014.9	88.5	
833	2013.6	166.3 E		880	0154.0	63.3	
834	2152.8	141.1		881	0333.2	38.1	
835	2332.0	116.0		882	0512.3	13.0 E	
836	0111.1	90.8		883	0651.5	12.2 W	
837	0250.3	65.6		884	0830.6	37.4	
838	0429.4	40.4		885	1009.8	62.5	
839	0608.6	15.3 E		886	1149.0	87.7	
840	0747.8	9.9 W		887	1328.1	112.9	
841	0926.9	35.0	30 May	888	1507.3	138.0	2 Jun
842	1106.1	60.2		889	1646.4	163.2 W	
843	1245.2	85.4		890	1825.6	171.6 E	
844	1424.4	110.6		891	2004.8	146.4	
845	1603.5	135.7		892	2143.9	121.3	
846	1742.7	160.9 W		893	2323.1	96.1	
847	1921.8	173.9 E		894	0102.2	70.9	
848	2101.0	148.8		895	0241.4	45.8	
849	2240.2	123.6		896	0420.5	20.6 E	
850	0019.3	98.4		897	0559.7	4.6 W	
851	0158.5	73.2	31 May	898	0738.8	29.8	3 Jun
852	0337.6	48.1		899	0918.0	54.9	
853	0516.8	22.9 E		900	1057.2	80.1	
854	0656.0	2.3 W		901	1236.3	105.3	
855	0835.1	27.4		902	1415.5	130.4	
856	1014.3	52.6		903	1554.6	155.6 W	
857	1153.4	77.8		904	1733.8	179.2 E	
858	1332.6	103.0		905	1912.9	154.1	
859	1511.7	128.1		906	2052.1	128.9	
860	1650.9	153.3		907	2231.2	103.7	
861	1830.0	178.4 W	908	0010.4	78.6		
862	2009.2	156.4 E	909	0149.6	53.4		
863	2148.4	131.2	910	0328.7	28.2		
864	2327.5	106.0	911	0507.9	3.0 E		
865	0106.7	80.9	912	0647.0	22.1 W		
866	0245.8	55.7	913	0826.2	47.3		
867	0425.0	30.5	914	1005.4	72.5		
868	0604.2	5.4 E	915	1144.5	97.6		
869	0743.3	19.8 W	916	1323.7	122.8		
870	0922.4	45.0	917	1502.8	148.0		
871	1101.6	70.2	918	1642.0	173.2 W		
872	1240.8	95.3	919	1821.1	161.7 E		
873	1419.9	120.5	920	2000.3	136.5		
874	1559.1	145.7	921	2139.4	111.3		
875	1738.2	170.8 W	922	2318.6	86.2		

Table A - (Continued)

<u>Pass Number</u>	<u>Time</u>	<u>Longitude</u>	<u>Date 1960</u>	<u>Pass Number</u>	<u>Time</u>	<u>Longitude</u>	<u>Date 1960</u>
923	0057.8	61.0	4 Jun	970	0638.1	42.0 W	7 Jun
924	0236.9	35.8		971	0817.2	67.2	
925	0416.1	0.6 E		972	0956.4	92.3	
926	0555.2	14.5 W		973	1135.6	117.5	
927	0734.4	39.7		974	1314.8	142.7	
928	0913.5	64.8		975	1453.9	167.8 W	
929	1052.7	90.0		976	1633.1	167.0 E	
930	1231.8	115.2		977	1812.2	141.8	
931	1411.0	140.4		978	1951.4	116.6	
932	1550.2	165.5 W		979	2130.6	91.5	
933	1729.3	169.3 E		980	2309.7	66.3	
934	1908.5	144.1		981	0048.9	41.1	
935	2047.6	119.0	982	0228.0	16.0 E		
936	2226.8	93.8	983	0407.2	9.2 W		
937	0006.0	68.6	984	0546.3	34.4		
938	0145.1	43.4	985	0725.5	59.6		
939	0324.2	18.3 E	986	0904.6	84.7		
940	0503.4	6.9 W	987	1043.8	109.9		
941	0642.6	32.1	988	1223.0	135.1		
942	0821.7	57.2	989	1402.1	160.2 W		
943	1000.9	82.4	990	1541.3	174.6 E		
944	1140.0	107.6	991	1720.4	149.4		
945	1319.2	132.8	992	1859.6	124.3		
946	1458.4	157.9 W	993	2038.7	99.1		
947	1637.5	176.9 E	994	2217.9	73.9		
948	1816.7	151.8	995	2357.0	48.8		
949	1955.8	126.6	996	0136.2	23.6 E	9 Jun	
950	2135.0	101.4	997	0315.4	1.6 W		
951	2314.1	76.2	998	0454.5	26.8		
952	0053.3	51.1	999	0633.7	51.9		
953	0232.4	25.9	1000	0812.8	77.1		
954	0411.6	0.7 E	1001	0952.0	102.3		
955	0550.8	24.4 W	1002	1131.2	127.4		
956	0729.9	49.6	1003	1310.3	152.6		
957	0909.1	74.8	1004	1449.4	177.8 W		
958	1048.2	100.0	1005	1628.6	157.0 E		
959	1227.4	125.1	1006	1807.8	131.9		
960	1406.5	150.3	1007	1946.9	106.7		
961	1545.7	175.5 W	1008	2126.1	81.5		
962	1724.8	159.4 E	1009	2305.2	56.4		
963	1904.0	134.2	1010	0044.4	31.2	10 Jun	
964	2043.2	109.0	1011	0223.6	6.0 E		
965	2222.3	83.8	1012	0402.7	19.1 W		
966	0001.5	58.7	1013	0541.9	44.3		
967	0140.6	33.5	1014	0721.0	69.5		
968	0319.8	8.4 E	1015	0900.2	94.6		
969	0458.9	16.8 W	1016	1039.3	119.8		

Table A - (Continued)

<u>Pass Number</u>	<u>Time</u>	<u>Longitude</u>	<u>Date 1960</u>	<u>Pass Number</u>	<u>Time</u>	<u>Longitude</u>	<u>Date 1960</u>
1017	1218.5	145.0 W	10 Jun	1064	1758.8	112.0 E	13 Jun
1018	1357.6	170.2 W		1065	1938.0	86.8	
1019	1536.8	164.7 E		1066	2117.1	61.7	
1020	1716.0	139.5		1067	2256.3	36.5	
1021	1855.1	114.3		1068	0035.4	11.4 E	14 Jun
1022	2034.3	89.2		1069	0214.6	13.8 W	
1023	2213.4	64.0		1070	0353.8	39.0	
1024	2352.6	38.8		1071	0532.9	64.2	
1025	0131.7	13.6 E	11 Jun	1072	0712.1	89.3	
1026	0310.9	11.5 W		1073	0851.2	114.5	
1027	0450.0	36.7		1074	1030.4	139.7	
1028	0629.2	61.9		1075	1209.6	164.8 W	
1029	0808.4	87.0		1076	1348.7	170.0 E	
1030	0947.5	112.2		1077	1527.9	144.8	
1031	1126.7	137.4		1078	1707.0	119.6	
1032	1305.8	162.5 W		1079	1846.2	94.5	
1033	1445.0	172.3 E		1080	2025.3	69.3	
1034	1624.1	147.1		1081	2204.5	44.1	
1035	1803.3	122.0		1082	2343.6	19.0 E	
1036	1942.4	96.8		1083	0122.8	6.2 W	15 Jun
1037	2121.6	71.6		1084	0302.0	31.4	
1038	2300.8	46.4		1085	0441.1	56.6	
1039	0039.9	21.3 E	12 Jun	1086	0620.3	81.7	
1040	0219.0	4.0 W		1087	0759.4	106.9	
1041	0358.2	29.1		1088	0938.6	132.1	
1042	0537.4	54.2		1089	1117.7	157.3 W	
1043	0716.5	79.4		1090	1256.9	177.6 E	
1044	0855.7	104.6		1091	1436.0	152.3	
1045	1034.8	129.8					
1046	1214.0	154.9 W					
1047	1353.2	179.9 E					
1048	1532.3	154.8					
1049	1711.5	129.6					
1050	1850.6	104.4					
1051	2029.8	79.2					
1052	2209.0	54.1					
1053	2348.1	28.9					
1054	0127.2	3.7 E	13 Jun				
1055	0306.4	21.4 W					
1056	0445.6	46.6					
1057	0624.7	71.8					
1058	0803.9	97.0					
1059	0943.0	122.1					
1060	1122.2	147.3					
1061	1301.4	172.5 W					
1062	1440.5	162.4 E					
1063	1619.6	137.2					

TABLE B - TIROS I POSITIONS AS FUNCTION OF TIME PAST ASCENDING NODE
(Approximated by a circular orbit)

<u>Time after A.N. (min)</u>	<u>Latitude (deg)</u>	<u>Increment (deg)</u>	<u>Longitude (deg East)</u>	<u>Increment (deg)</u>
0	00.0		00.0	
1	2.7	2.7	02.1	2.1
2	5.4	2.7	04.3	2.2
3	8.1	2.7	06.5	2.2
4	10.8	2.7	08.7	2.2
5	13.5	2.7	11.0	2.3
6	16.2	2.7	13.3	2.3
7	18.9	2.7	15.7	2.4
8	21.5	2.6	18.2	2.5
9	24.0	2.5	20.8	2.6
10	26.5	2.5	23.5	2.7
11	28.9	2.4	26.3	2.8
12	31.3	2.4	29.2	2.9
13	33.5	2.2	32.3	3.1
14	35.7	2.2	35.6	3.3
15	37.8	2.1	39.1	3.5
16	39.7	1.9	42.8	3.7
17	41.5	1.8	46.6	3.8
18	43.2	1.7	50.7	4.1
19	44.7	1.5	55.0	4.3
20	45.9	1.2	59.6	4.6
21	47.0	1.1	64.4	4.8
22	47.8	0.8	69.3	4.9
		0.6		5.1

TABLE B - (Continued)

<u>Time after A.N. (min)</u>	<u>Latitude (deg)</u>	<u>Increment (deg)</u>	<u>Longitude (deg East)</u>	<u>Incremen (deg)</u>
23	48.4		74.4	
		0.3		5.1
24	48.7		79.5	
		0.1		4.2
24.8	48.8		83.7	
		0.0		1.0
25	48.8		84.7	
		0.2		5.2
26	48.6		89.9	
		0.4		5.1
27	48.2		95.0	
		0.7		5.0
28	47.5		100.0	
		0.9		4.9
29	46.6		104.9	
		1.2		4.7
30	45.4		109.6	
		1.4		4.5
31	44.0		114.1	
		1.5		4.2
32	42.5		118.3	
		1.7		4.0
33	40.8		122.3	
		1.9		3.8
34	38.9		126.1	
		1.9		3.6
35	37.0		129.7	
		2.1		3.4
36	34.9		133.1	
		2.2		3.2
37	32.7		136.3	
		2.4		3.1
38	30.3		139.4	
		2.3		2.9
39	28.0		142.3	
		2.5		2.7
40	25.5		145.0	
		2.5		2.6
41	23.0		147.6	
		2.5		2.6
42	20.5		150.2	
		2.7		2.5
43	17.8		152.7	
		2.6		2.4
44	15.2		155.1	
		2.7		2.3

TABLE B - (Continued)

<u>Time after A.N. (min)</u>	<u>Latitude (deg)</u>	<u>Increment (deg)</u>	<u>Longitude (deg East)</u>	<u>Increment (deg)</u>
45	12.5		157.4	
		2.6		2.2
46	09.9		159.6	
		2.7		2.2
47	07.2		161.8	
		2.8		2.2
48	04.4		164.0	
		2.7		2.1
49	01.7		166.1	
		1.7		1.3
49.6	00.0		167.4	
		1.0		0.9
50	-01.0		168.3	
		2.8		2.1
51	-03.8		170.4	
		2.7		2.2
52	-06.5		172.6	
		2.7		2.2
53	-09.2		174.8	
		2.7		2.2
54	-11.9		177.0	
		2.7		2.3
55	-14.6		179.3	
		2.6		2.4
56	-17.2		181.7	
		2.7		2.4
57	-19.9		184.1	
		2.5		2.5
58	-22.4		186.6	
		2.5		2.6
59	-24.9		189.2	
		2.5		2.7
60	-27.4		191.9	
		2.4		2.9
61	-29.8		194.8	
		2.3		3.0
62	-32.1		197.8	
		2.3		3.2
63	-34.4		201.0	
		2.1		3.4
64	-36.5		204.4	
		2.0		3.5
65	-38.5		207.9	
		1.9		3.7
66	-40.4		211.6	
		1.7		4.0

TABLE B - (Continued)

<u>Time after A.N. (min)</u>	<u>Latitude (deg)</u>	<u>Increment (deg)</u>	<u>Longitude (deg East)</u>	<u>Increment (deg)</u>
67	-42.1		215.6	
		1.7		4.2
68	-43.8		219.8	
		1.4		4.4
69	-45.2		224.2	
		1.1		4.6
70	-46.3		228.8	
		1.0		4.8
71	-47.3		233.6	
		0.7		5.0
72	-48.0		238.6	
		0.5		5.1
73	-48.5		243.7	
		0.3		5.2
74	-48.8		248.9	
		0.0		2.3
74.4	-48.8		251.2	
		0.1		2.9
75	-48.7		254.1	
		0.2		5.2
76	-48.5		259.3	
		0.6		5.1
77	-47.9		264.4	
		0.7		5.0
78	-47.2		269.4	
		1.0		4.8
79	-46.2		274.2	
		1.2		4.6
80	-45.0		278.8	
		1.4		4.4
81	-43.6		283.2	
		1.7		4.1
82	-41.9		287.3	
		1.8		3.9
83	-40.1		291.2	
		1.9		3.8
84	-38.2		295.0	
		2.0		3.5
85	-36.2		298.5	
		2.1		3.3
86	-34.1		301.8	
		2.3		3.1
87	-31.8		304.9	
		2.4		3.0
88	-29.4		307.9	
		2.4		2.9

TABLE B - (Continued)

<u>Time after A.N. (min)</u>	<u>Latitude (deg)</u>	<u>Increment (deg)</u>	<u>Longitude (deg East)</u>	<u>Increment (deg)</u>
89	-27.0	2.4	310.8	2.7
90	-24.6	2.5	313.5	2.6
91	-22.1	2.6	316.1	2.5
92	-19.5	2.7	318.6	2.4
93	-16.8	2.6	321.0	2.3
94	-14.2	2.7	323.3	2.3
95	-11.5	2.7	325.6	2.2
96	-08.8	2.7	327.8	2.2
97	-06.1	2.7	330.0	2.2
98	-03.4	2.8	332.2	2.1
99	-00.6	0.6	334.3	0.6
99.2	00.0		334.9	

TIROS I- ORIENTATION NOMOGRAM

U S DEPARTMENT OF COMMERCE
WEATHER BUREAU
MSL REPORT NO. 5

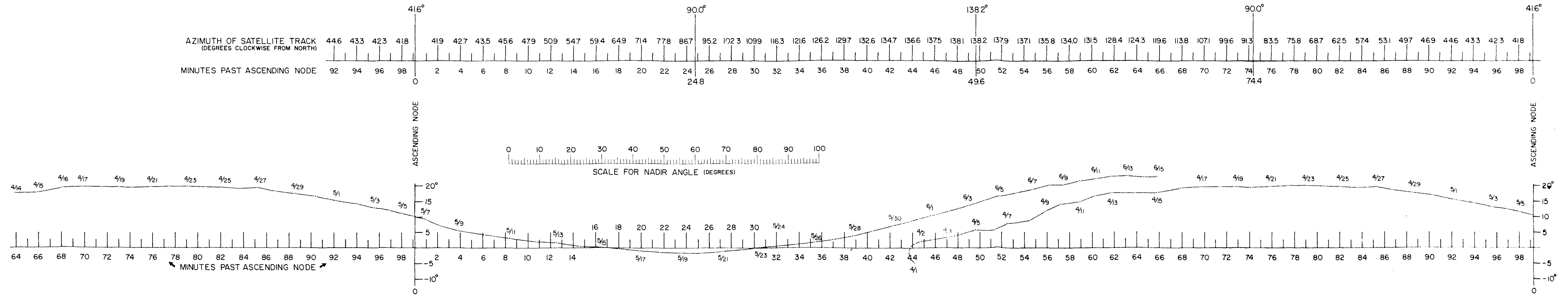


Figure 2. Nomogram for computing azimuth of the principal plane and nadir angle of the optical axis. Points are for 1200 GCT each day April 1 to June 15, 1960.